Artificial Intelligence Research and Applications (AIra)
https://www.ijaira.org/ Online ISSN: 3108-3889
A. Milles et al., Vol. 2, No. 1, March, 2026 Research Article

Neural Networks-Based 12-Sector Direct Torque Control of Asynchronous Machine Drives: Experimental Results

Abdessmad Milles *, Habib Benbouhenni **‡, Adil Yahdou ***, Nicu Bizon*****

* University of Bordj Bou-Areridj, Algeria.
** Department of Electrical Engineering, Faculty of Technology, Hassiba Benbouali University of Chlef, Chlef, Algeria.
*** University of Chlef, Chlef, Algeria.
**** The National University of Science and Technology Politehnica Bucharest, Pitești University Centre, 110040 Pitesti, Romania.
(abdessmad.milles@univ-bba.dz, habib0264@gmail.com, a.yahdou@univ-chlef.dz, nicu.bizon1402@upb.ro)

‡Corresponding Author: Habib Benbouhenni, Department of Electrical Engineering, Faculty of Technology, Hassiba Benbouali University of Chlef, Chlef, Algeria, habib0264@gmail.com.

Received: 12.10.2025, Revised: 14.11.2025, Accepted: 18.01.2026

Abstract- Achieving optimal performance from industrial asynchronous motors requires precise control of both torque and magnetic flux. The conventional six-sector direct torque control (6-DTC) method is widely used for this purpose, but it suffers from several drawbacks, including significant torque and flux ripple and excessive switching activity in the power converter, which leads to energy losses. This research addresses these issues by introducing an enhanced control method that integrates neural networks (NNs) with a refined twelve-sector direct torque control (12-DTC) scheme. Unlike traditional approaches that depend on hysteresis comparators and fixed lookup tables, the proposed NN-based controller intelligently determines voltage vectors in real time, enabling smoother and more adaptive motor operation. Simulation studies verified the method's effectiveness, showing substantial reductions in torque ripple, improved control tracking, and lower total harmonic distortion (THD). Experimental validation on a dSPACE DS1104 hardware platform confirmed these improvements in practice. The 12-sector NN-DTC achieved THD reductions of 30.87%, 42.22%, and 49.73% across different test conditions, along with 47% faster dynamic speed response. Overall, the proposed neural network–based 12-sector DTC represents a significant advancement over the traditional 6-DTC. It delivers smoother performance, more rapid response, higher efficiency, and robust real-world applicability—offering a more precise and energy-efficient solution for controlling industrial asynchronous machines.

Keywords: Neural networks, asynchronous machine, direct torque control, 12-sector DTC, torque ripple, THD reduction.

1. Introduction

Advancements in highly efficient technologies have expanded the range of applications for electrical machines (EMs) within industrial settings, including the asynchronous machine (AM). Numerous researchers in the literature have proposed various approaches for controlling these types of EMs, such as the conventional direct torque control (DTC) and field-oriented control (FOC) [1, 2].

The DTC approach involves directly selecting the inverter's switching states through a predefined switching

Cite this article as: A. Milles, H. Benbouhenni, A. Yahdou, and N. Bizon, "Neural Networks-Based 12-Sector Direct Torque Control of Asynchronous Machine Drives: Experimental Results," *Artificial Intelligence Research and Applications (AIra)*, Vol. 2, No. 1, pp. 1–31, March, 2026, https://doi.org/10.20508/qyxvy507.

table (ST), offering advantages like a simple structure and rapid response when compared to the FOC strategy. However, the basic DTC technique relies on hysteresis comparators (HCs) that operate with variable switching frequencies (SFs), leading to significant torque and flux ripples that can negatively impact the performance of the AM [3-5].

To address the limitations of the conventional DTC technique, many researchers have suggested enhancements that maintain a constant SF and minimize torque and flux ripples. One of the designed solutions is the application of space vector modulation (SVM) to the DTC strategy, which effectively manages the SF and minimizes flux, torque, and current fluctuations.

The SVM-DTC approach replaces HCs with proportional-integral (PI) regulators to produce the reference voltage components [6]. Although this algorithm significantly improves performance, it requires precise information about the system's parameters [7].

In [8], sliding mode controllers (SMCs) were introduced as a substitute for linear PI regulators to achieve a more robust and nonlinear control. This approach offers strong dynamic performance and high resilience to external disturbances. However, a major disadvantage of this technique is the phenomenon known as "chattering," which restricts the motor's operational range. Table 1 presents various studies that address the drawbacks of applying the DTC technique to the rotor speed control of an AM.

In the literature, various studies have utilized AMs in renewable energy (RE) systems. Reference [16] describes the design of a wind turbine (WT) emulator using a squirrel-cage AM and a separately excited direct current machine to emulate WT behavior in a laboratory environment. The system incorporates user-friendly software for selecting wind data and WT models, alongside hardware for real-time control and monitoring. Key components include a PI-controlled AM, a non-isolated step-up converter supporting maximum power point tracking (MPPT), and a load simulator for evaluating efficiency under variable conditions. The emulator facilitates the testing of small-scale wind systems while providing comprehensive electrical and mechanical data monitoring. However, the study focuses primarily on design and simulation, with limited exploration of advanced control strategies or thorough experimental validation under diverse environmental conditions, which may restrict its broader applicability.

In the work of Ghizlane et al. [17], a photovoltaic-powered water pumping system was designed, utilizing a three-phase AM controlled through a sinusoidal PWM (SPWM) technique. The system incorporates a DC-DC boost converter managed by a perturb-and-observe MPPT algorithm to optimize energy extraction from the photovoltaic array. A PI controller adjusts the SPWM frequency to regulate the motor speed according to the calculated reference speed, ensuring operation at maximum efficiency. MATLAB/Simulink simulations were performed to test the system under varying climatic conditions, demonstrating the PI regulator's effectiveness in maintaining motor speed and extracting maximum power. The study emphasizes the importance of integrating RE sources for sustainable water pumping solutions. However, the approach experiences torque oscillations during climatic variations, indicating a need for more advanced control strategies or improved tuning of the PI regulator to ensure smoother operation.

In [18], a single-phase induction motor is proposed to be powered by a solar system, using a DTC strategy to control the operation of this machine. Additionally, a matrix-type power converter is used to change the motor speed and manage the inverter output voltage. Using this converter allows for significant improvements in current and torque quality compared to a conventional inverter. This proposed strategy has been implemented in the MATLAB environment, and the results demonstrate the effectiveness of the designed approach in improving the quality of current and torque compared to the traditional approach. The drawback of the proposed approach lies in the use of a matrix converter, which is characterized by complexity, high costs, and difficulty in implementation.

In the work by Masood et al. [19], a variable frequency drive (VFD) was proposed to address frequency fluctuations in micro-hydro power plants caused by variations in water flow and consumer load. The system integrates an electronic governor using a variable-speed AM to consume excess generated power, enabling its use for irrigation or water storage. The VFD converts the variable-frequency AC output of the micro-hydro system into a stable 50 Hz AC signal through AC-DC-AC conversion. Additionally, the design includes a DC bus that supports integration with other renewable energy sources, such as solar or fuel cells, enhancing system scalability. The study validates the VFD and electronic governor under various load and water flow conditions, demonstrating improved frequency stabilization. However, the proposed system's economic feasibility in large-scale applications remains unclear, particularly concerning the costs of integrating additional renewable energy sources and maintaining the motor as a secondary load.

In [20], a hybrid combination of the SPWM technique and PI regulator is proposed to enhance the performance of a single-phase AM (1-phase AM) powered by solar energy. The research emphasizes the importance of improving electricity quality in smart grids, particularly through harmonic analysis. The authors implemented a matrix converter alongside a multistage power conversion system, which includes a boost converter and a PV module, to optimize speed and voltage. The THD of the input voltage was analyzed, revealing a significant improvement with the proposed model, achieving a THD of 3.5 % compared to traditional methods.

Additionally, the perturb and observed MPPT technique was utilized to maximize energy extraction from the photovoltaic system. However, a notable con of this approach is the complexity involved in the hardware implementation and the potential challenges in real-time adjustments during varying operational conditions.

Table 1. Some works addressing the limitations of the conventional DTC strategy

Techniques	Type of validation	Pros	Cons
Twelve sectors DTC technique using backstepping speed control [9].	Simulation and experimental.	- Reduced torque and flux ripples for improved stability. - Enhanced speed tracking with robust backstepping control (BC). - Reduced total harmonic distortion (THD) in stator currents. - Effective stator resistance estimation using P-model reference adaptive control (MRAC). - Validated improvements through simulations and experiments.	- Increased computational complexity with the twelve-sector DTC approach. - Dependence on precise parameter identification. -Hardware realization requires high-performance processing. - Limited analysis of scalability for larger systems.
Ant colony optimization (ACO) algorithm-DTC technique [10].	Experimental.	- Integration of ACO algorithm to enhance PI controller performance in DTC systems. - Improved flux and torque fluctuation reduction compared to DTC technique. - Enhanced system robustness against nonlinearity and parameter variations. -Experimentally validated gains in speed tracking and system stability. - Reduction in THD of stator and rotor currents.	- High computational demand for ACO algorithm. - Dependence on precise parameter tuning for optimal PI controller performance. - Limited exploration of scalability for industrial applications. - Increased complexity for real-time implementation on low-resource hardware.
Fractional-order SMC (FOSMC) technique [11].	Simulation.	- The FOSMC technique outperforms traditional PI and SMC controllers in AM control, offering superior robustness, reduced overshoot, faster response, minimized chattering, and adaptive design for dynamic conditions.	- While FOSMC technique improves control performance, it introduces design complexity, requires adaptive tuning, and depends on accurate system modeling, with challenges like residual chattering and performance sensitivity under extreme conditions.
Duty ratio control technique [12].	Simulation and experimental.	- The paper presents a simplified duty ratio control technique that minimizes torque and current ripples, enhancing performance in DTC drives. - It retains the simplicity of traditional ST-based DTC algorithms, making it easier to implement. - The proposed method utilizes parallel low-speed control loops, reducing computational burden and eliminating the need for delay compensation. - By modulating the duty ratio based on torque error, the technique effectively improves the overall efficiency of AM drives in electric vehicles.	- The paper does not address potential limitations in the modified duty ratio control algorithm, such as its dependency on accurate torque error measurement. - The complexity of the control algorithm may still pose challenges in real-time applications, despite efforts to simplify it. - The reliance on lookup tables for duty ratio modulation could introduce additional computational overhead in certain scenarios. - The proposed method may not fully eliminate torque and current ripples, especially under varying load conditions.
Novel reference flux selection technique [13].	Simulation.	- Introduces a novel reference flux selection algorithm to reduce torque fluctuation in AMs for electric vehicles. - Demonstrates improved performance over conventional DTC methods. - Achieves significant reductions in torque ripple and current THD. -Validated through simulations using a 50-hp AM, ensuring practical applicability. - Contributes to energy efficiency, reducing battery energy consumption by 37.3% compared to classical DTC technique.	- Limited to simulation results, lacking real-world experimental validation. - Focuses primarily on torque ripple, potentially overlooking other performance metrics. - May require complex implementation in practical applications. - Assumes ideal conditions that may not reflect all operational scenarios. - The proposed method's scalability to larger systems is not addressed.

Table 1. *cont.*

Fuzzy second-order SMC (FSOSMC) optimized by genetic algorithm (GA) [14].	Simulation.	- The FSOSMC technique enhances control performance, reduces torque ripples, improves robustness against disturbances, minimizes chattering, and optimizes parameters using GA techniques for dual star AMs.	- The paper does not address potential complexities in implementing FSOSMC technique, reliance on GA techniques may introduce computational overhead, and variable SF issues remain unresolved.
Multi-level inverter [15].	Simulation.	- The paper analyzes losses in dual-inverter-fed open-end winding AM drives, introducing an improved loss model, comparing pulse width modulation (PWM) schemes, and highlighting significant efficiency gains with DPWM technique for safer, reliable operation.	- The paper's limitations include lacking experimental validation, focusing solely on dual inverter systems, model complexity, limited environmental impact discussion, and narrow exploration of PWM techniques, restricting broader applicability and practicality.

In the field of control, the DTC strategy is one of the most prominent linear strategies used to control electrical machines [21]. This strategy has several advantages that make it a promising solution for controlling electrical machines, especially AM. This strategy relies on estimating both torque and flux [22]. The strategy aims to make torque vary directly with current, making the machine similar in principle to a direct current machine [23]. Therefore, this strategy is of great importance in the field of control, as evidenced by the number of works that have addressed it. This strategy has several drawbacks that limit its spread, the most prominent of which are low robustness and high torque and flux ripples [24]. Furthermore, the high THD of the current is another major drawback of this strategy.

Several solutions have been proposed to overcome the problems of the DTC strategy, the most prominent of which is replacing both ST and HC with other more, efficient strategies. In [25], a new strategy is proposed for the DTC technique of an induction motor. This designed strategy relies on the use of a dual PI controller to control the flux and torque, where the outputs of these controllers are reference voltage values. The modified SVM strategy is used to compensate for the use of ST in controlling the machine's inverter. This designer is designed for simplicity, fast dynamics, and excellent performance. The MATLAB Neo environment was used, along with the Liberals, and the results showed that the designer achieved an excellent THD value of 28.57 % compared to the traditional DTC approach.

A fuzzy super-twisting SMC technique is the proposed solution in [26] to overcome the problems and drawbacks of the DTC strategy of the induction generator. This designed controller is characterized by high robustness and excellent performance, as it uses two controllers to control the flux and torque. In addition to using this designed controller, the modified SVM strategy is used to generate the pulses necessary to operate the machine's inverter. This strategy was compared to the DTC-based PI controller approach. Compared to the DTC-PI strategy, the proposed approach is more complex and expensive. The MATLAB environment was used to implement this proposed approach under various operating conditions, and the results showed that the proposed approach significantly reduced torque/flux ripples compared to the DTC-PI strategy. Furthermore, the proposed approach reduced the THD of the current by approximately 61.54% and 46.55% in all tests compared to the DTC-PI approach. Despite this remarkable performance, there is a drawback to this proposed approach. It features a significant number of gains, making it difficult to fine-tune the dynamic response to torque and flux. Furthermore, the use of fuzzy logic (FL) makes it difficult to easily fine-tune the control, given the lack of a mathematical rule that specifies the number of rules required to achieve optimal performance. As is well known, the FL method relies heavily on experience, requiring experimentation and iteration to achieve optimal results.

An adaptive network-based fuzzy inference system is combined with the second-order super-twisting sliding mode (STSM) algorithm [27] to obtain a robust controller that overcomes the DTC problem. In this designed approach, a modified SVM strategy is used along with the proposed controller to develop the DTC strategy. The proposed DTC strategy is characterized by high robustness, high efficiency, ease of implementation, and fast dynamic response. This proposed DTC strategy uses the same torque and flux estimation equations as the traditional approach. The proposed strategy was implemented in MATLAB using several different tests, comparing its performance and effectiveness with the DTC-PI approach. The results showed that the designed approach reduced the THD of current by 61.54 % and 57.33 % percent compared to the DTC-PI approach. Furthermore, the designed approach yielded better results compared to DTC-PI in terms of reference tracking and reduced torque/flux ripples. This approach has drawbacks, the most notable of which are its complexity and the presence of a significant number of gains. This designed approach is affected by changes in machine parameters in robustness testing, manifested in increased torque/flux ripples and higher THD of current, necessitating the search for a more effective and high-performance strategy.

In [28], an FL method-based DTC technique is proposed for synchronous motor control. The FL method is used to compensate for the controller's PI of speed, and 25 FL rules are used to embody the FL controller. In this designed

strategy, ST is used to control an inverter. This designed strategy is compared with a conventional approach, implemented using MATLAB/SIMULINK. The effectiveness of the designed approach is verified under different speeds and load disturbances. The obtained results demonstrate the effectiveness of the proposed control in reducing torque and current ripples at different speeds while improving the dynamic response to speed and flux.

In [29], a new DTC strategy is proposed for controlling an induction machine. This strategy is a neural network (NN)-based discrete predictive direct torque and flux control (NNPDTFC). This strategy uses the SVM technique to drive the machine inverter, which makes it different from the conventional approach that uses both ST and HC. The performance and effectiveness of the proposed approach are compared with a DTC strategy based on PI controllers. In this work, the gain values of the proposed approach were calculated using the particle swarm optimization algorithm. Minimized disturbances, simple control, and real-time implementation are key features of the designed approach, which also enhances the transient performance of the motor drive by reducing settling time and peak overshoot. The performance of the designed approach was analyzed using MATLAB. The obtained results show that the proposed approach significantly improves the flux and torque ripples compared to the conventional PI controller-based approach. Furthermore, this designed approach was experimentally implemented using a low-cost digital signal processor (DSP) controller, where a 3.7 kW induction motor was used. Experimentally, the designed approach yielded highly satisfactory results under uncertain system parameters and external load disturbances. Furthermore, it yielded enhanced dynamic performance as well as static performance with reduced ripples in signal flux, torque, and current compared to the conventional PI controller-based approach.

Another strategy proposed in [30] for controlling an induction motor is the DTC based on a decision tree (T-DTC), which uses actively trained artificial NNs (ANNs) to enhance accuracy and robustness. The goal of the T-DTC strategy proposal is to significantly reduce flux and torque ripples, ensuring efficient control of induction motors. Conventional stator flux and electromagnetic torque hysteresis controllers have been replaced with two advanced controllers known as M5 Prime model trees. Additionally, the conventional switching table has been replaced with a new decision tree using the classification algorithm 4.5. The effectiveness of the proposed T-DTC strategy was demonstrated using MATLAB/Simulink, comparing the performance with the conventional approach. Several different tests were used. The validity and efficiency of this approach were also validated in real-time using the HIL platform based on the OPAL-RT OP 5600 and the Virtex 6 FPGA ML605. The results show that the proposed approach offers a significant improvement over existing techniques in the literature, making it a promising solution. One of the most prominent solutions proposed to overcome the problems of the DTC strategy is the use of NNs as a suitable solution due to their accuracy and ease of use [31]. In [32], an NN technique was used to improve the properties of the DTC strategy of a permanent magnet synchronous motor (PMSM). This strategy is different from the traditional strategy, as its use allows for reducing torque ripples. Moreover, the use of this strategy allows for a lower value of the THD of the current compared to the traditional approach.

Another work in [33] addressed the application of the ANN strategy to overcome the problems of the DTC technique of induction motor. In this work, ANN techniques were used to compensate for both HC and ST of the DTC technique. The designed strategy is characterized by fast dynamic response, high robustness, and ease of implementation. The results obtained showed the high performance of the designed approach compared to the conventional approach in terms of torque/current ripples and THD value of current. In [34], the adaptive NN approach was proposed to overcome the DTC strategy problems of linear induction motor drives. This strategy was implemented in the MATLAB environment using various tests. The results demonstrated the effectiveness and efficiency of the adaptive NN approach in improving the operational performance of DTC. In [35], the neural DTC technique of the induction motor was experimentally implemented using an FPGA. After giving the mathematical model of the induction motor and the equations expressing the DTC approach, the designed approach was experimentally implemented using an FPGA. The results of the tests conducted prove the effectiveness of the designed approach in improving the performance and efficiency of the machine when using the neural DTC approach compared to the traditional technique.

In [36], deep reinforcement learning is used to improve the DTC strategy properties of PMSM with parameter robustness. The use of deep reinforcement learning improves the operational performance of the DTC approach and increases its robustness. The MATLAB environment is used to verify the effectiveness of the designed approach. Various tests are performed, and the results are compared with the traditional strategy. Simulation results show that the use of DTC reduces flux/torque ripples and significantly reduces the THD of current compared to the traditional DTC technique. FL technique was combined with NN techniques in [37] to create a robust controller that overcomes the drawbacks of the DTC strategy. The author used a three-level inverter to power the machine. Furthermore, to improve the performance of the DTC strategy, 24 sectors were used instead of the usual six. In this designed strategy, an NN-FL controller was used to control both flux and torque. ST was also used to generate the pulses required to drive a three-level inverter. MATLAB was used to implement the designed approach and compare its performance with the conventional approach under various operating conditions. Simulation results demonstrated the superior performance of the designed approach, reducing the THD of current by 77.50%, 48.34%, 75%, and 81.43% compared to the conventional approach. Furthermore, torque ripples were reduced by 30%, 39.24%, 31.94%, and 59.31% compared to the conventional approach. Despite this performance, the designer's approach has drawbacks, the most significant of which lies in its use of ST and torque/flux estimation, which significantly impacts machine parameter changes.

This experimental work proposes to study the effectiveness of using an NN controller to overcome the drawbacks of the 12-sector DTC (12-DTC) algorithm applied to AM while comparing the results with the 6-sector DTC (6-DTC) technique. Therefore, the main contribution of the paper lies in the application of NN techniques to overcome the problems of the 12-sector DTC algorithm. This strategy is a modification and development of the 6-DTC technique. In this designed algorithm, NNs are used to compensate for both HC and ST. The 12 sectors neural DTC strategy is a different strategy, as it differs from related businesses such as [29] and [30] in terms of principle, simplicity, and ease of implementation. First, this algorithm is tested using MATLAB, and the results are compared with the traditional approach. Various tests were used to prove the effectiveness and efficiency of applying NNs. All tests demonstrated the strength of the algorithm in reducing torque ripples and reducing the THD of the current. Secondly, the simulated results were confirmed using real tools, where the dSPACE 1104 was used to control the operation of the 3.5 kW AM drive. Therefore, implementing the proposed algorithm using real equipment is considered the second main contribution of this paper. The obtained experimental results confirm the simulation results, making the proposed approach applicable in various industrial fields such as electric vehicles and electric power generation. Experimentally, the proposed 12-sector neural DTC (12-NDTC) algorithm, compared to the traditional approach, has high competence and great efficacy, as the torque and flux ripples are reduced. Also, this proposed algorithm improved the speed response time value and the THD value of the current compared to the 6-DTC technique. In addition to these experimental results obtained, the designed algorithm is simple, easy to realize, and inexpensive. Accordingly, the objectives achieved from this paper can be extracted in the form of the following points:

- Experimentally verify the effectiveness of applying NNs in overcoming DTC technique defects.
- Significantly improve dynamic speed response.
- Significantly underestimates the THD of the current compared to the 6-DTC technique.
- Reduce stator flux fluctuations.
- Reducing the value of exceeding the speed limit compared to the traditional approach.
- Reduce torque and current fluctuations.
- Increasing the robustness and efficacy of the AM control system compared to using the 6-DTC technique.

The sections of the article are as follows: The second section deals with the AM model. In the third section, the 12 sectors DTC approach algorithm is discussed in detail, mentioning the pros and cons. 12 sectors neural DTC algorithm are listed in Section IV. In Section V, a simulation of the designed algorithm using MATLAB is discussed. In the sixth section, the suggested algorithm was realized using experimental work (dSPACE 1104), where real tools were used to implement it. In Section VII, all conclusions of the work are listed.

2. AM Model

In this section, the mathematical model (MM) of AM used in this work is discussed. To give the model, the Concordia transform is used. This conversion is based on simplifying the machine model, where mathematical equations are given for each part of the machine. This model has been detailed in several scientific works [38, 39]. Equation (1) represents the AM voltages in the axis (αβ).

$$\begin{cases} V_{\alpha s} = R_s I_{\alpha s} + \dfrac{d}{dt}\Phi_{\alpha s} \\ V_{\beta s} = R_s I_{\beta s} + \dfrac{d}{dt}\Phi_{\beta s} \\ V_{\beta r} = R_r I_{\beta r} + \dfrac{d}{dt}\Phi_{\beta r} - w\Phi_{\alpha r} \\ V_{\alpha r} = R_r I_{\alpha r} + \dfrac{d}{dt}\Phi_{\alpha r} + w\Phi_{\beta r} \end{cases} \quad (1)$$

The rotor currents in the axis (αβ) can be written by Equation (2). This equation was obtained based on Equation (1).

$$\begin{cases} I_{\alpha r} = \dfrac{\Phi_{\alpha s} - L_s I_{\alpha s}}{M_{sr}} \\ I_{\beta r} = \dfrac{\Phi_{\beta s} - L_s I_{\beta s}}{M_{sr}} \end{cases} \quad (2)$$

From Equation (1), the expression for the flux in the αβ axis can be extracted according to Equation (3) [40].

$$\begin{cases} \Phi_{\alpha r} = \dfrac{L_r}{M_{sr}}(\Phi_{\alpha s} - \sigma L_s I_{\alpha s}) \\ \Phi_{\beta r} = \dfrac{L_r}{M_{sr}}(\Phi_{\beta s} - \sigma L_s I_{\beta s}) \end{cases} \quad (3)$$

Derivation of Equation (3) allows writing Equation (4). This equation is used to create an AM model in MATLAB.

$$\begin{cases} \dfrac{d\Phi_{\alpha r}}{dt} = \dfrac{L_r}{M_{sr}}\left(\dfrac{d\Phi_{\alpha s}}{dt} - \sigma L_s \dfrac{dI_{\alpha s}}{dt}\right) \\ \dfrac{d\Phi_{\beta r}}{dt} = \dfrac{L_r}{M_{sr}}\left(\dfrac{d\Phi_{\beta s}}{dt} - \sigma L_s \dfrac{dI_{\beta s}}{dt}\right) \end{cases} \quad (4)$$

The torque of the AM is calculated according to the Equation (5). To change the torque, it is enough to change the current or flux.

$$T_e = \frac{pM_{sr}}{L_r}(\Phi_{\alpha r} I_{\beta s} - \Phi_{\beta r} I_{\alpha s}) \quad (5)$$

Equation (6) shows the relationship between speed and torque. Through this relationship, the operation of the AM and the rotational speed can be controlled.

$$J\frac{d\Omega_r}{dt} = T_e - T_r - f_r\Omega_r \quad (6)$$

In the next section, a 12-sector DTC approach is proposed for AM control instead of using the traditional algorithm. In this section, the operating principle will be given, mentioning the cons and pros.

3. 12 Sectors DTC Algorithm

The 12-DTC algorithm is considered one of the most prominent solutions designed to defeat the problems of the conventional DTC algorithm [41]. Its use allows for a significant increase in competence and robustness. This approach is a modification and development of the conventional DTC algorithm. In the 12-DTC algorithm, a four-level HC is used to control torque, and a 2-level HC is used to control flux. Also, in the 12-DTC algorithm an ST is used to control the inverter of the AM [42]. Therefore, the 12-DTC algorithm is described by its simplicity, ease of implementation, satisfactory performance, low costs, and fast dynamic response [43].

The 12-DTC algorithm is listed in Figure 1, which has the same structure as the traditional algorithm. In this algorithm, estimation of both torque and flux is used, which is a necessary process to calculate the torque and flux error. Also, the PI controller is used to calculate the torque reference value. The input to this regulator is the speed error and its output is the torque reference value. This controller was relied upon for its simplicity, ease of operation, fast dynamic response, and ease of adjustment.

In the 12-DTC algorithm, both voltage and current are measured to estimate torque and flux. In this algorithm, no sensors are used to capture speed, which makes it easy to maintain, inexpensive, and highly accurate.

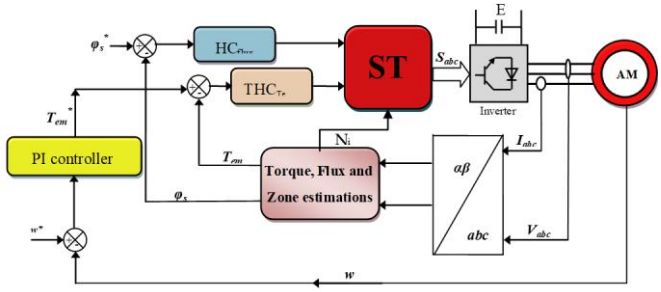

Fig. 1. 12-DTC algorithm of AM.

Table 2. The ST of 12-DTC algorithm

N_i		1	2	3	4	5	6	7	8	9	10	11	12
HC flux	HC torque												
0	2	3	4	4	5	5	6	6	1	1	2	2	3
	1	4	4	5	5	6	6	1	1	2	2	3	3
	-1	7	5	0	6	7	1	0	2	7	3	0	4
	–2	5	6	6	1	1	2	2	3	3	4	4	5
1	2	2	3	3	4	4	5	5	6	6	1	1	2
	1	2	2	3	3	4	4	5	5	6	6	1	1
	-1	1	1	2	2	3	3	4	4	5	5	6	6
	–2	6	1	1	2	2	3	3	4	4	5	5	6

To produce the pulses necessary to run the inverter, Table 2 is used, which contains 12 sectors [42]. This table is larger than the ST of the traditional algorithm, which gives it greater efficiency. Changes in flux, sector, and torque make it possible to select voltage vectors to follow torque and flux reference values. ST is the basic element in the DTC algorithm, and the selection of efforts plays an important role in the efficiency and performance of this algorithm.

Figure 2 represents the HC used to control torque. This regulator has the following outputs: 2, -2, 1, and -1 [43]. Outputs with negative values are used to be able to reverse the rotation direction of the AM. Figure 3 represents the HC proposed in this algorithm for flux control. Therefore, this HC has two states: 0 and 1 [41]. The strategy depends on measuring voltage and current, and to calculate these values in axis (αβ), Equation (7) is used for this purpose.

$$\begin{bmatrix} V_{\alpha s} \\ V_{\beta s} \end{bmatrix} = \frac{2}{3}\begin{bmatrix} 1 & -1/2 & -1/2 \\ 0 & \sqrt{3}/2 & -\sqrt{3}/2 \end{bmatrix}\begin{bmatrix} V_{sa} \\ V_{sb} \\ V_{sc} \end{bmatrix} \quad (7)$$

The DTC algorithm is characterized by three errors: flux error, torque error, and speed error ($\varepsilon_{\Phi s}$, ε_{Te}, and ε_{Ω}). In addition to the angle θ_s that determines the location of the vector Φ_s based on the components $\Phi_{s\alpha}$ and $\Phi_{s\beta}$. Equation (8) shows the errors used in the DTC algorithm [44].

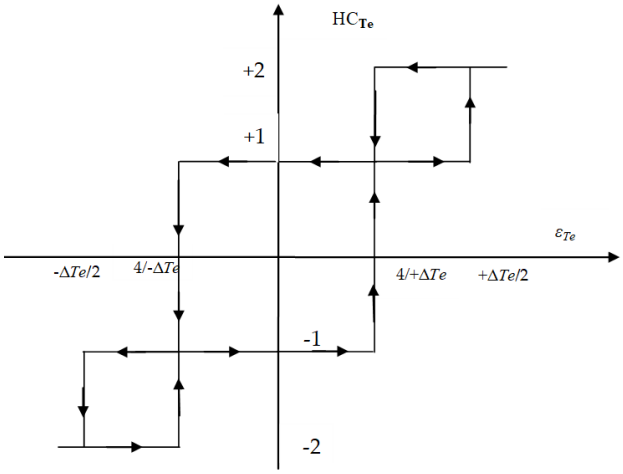

Fig. 2. Torque HC regulator.

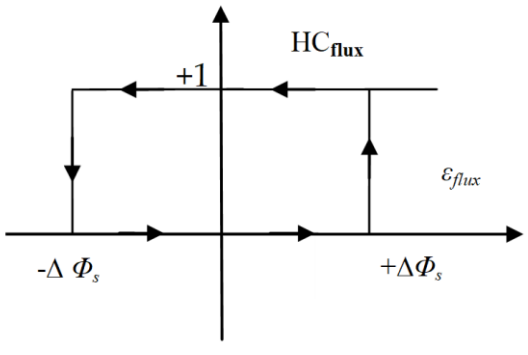

Fig. 3. Flux HC regulator.

$$\begin{cases} \varepsilon_{\Phi_S}=\Phi_S^*-\Phi_S \\ \varepsilon_{T_e}=T_e^*-T_e \\ \varepsilon_{\Omega}=\Omega^*-\Omega \end{cases} \quad (8)$$

Equation (9) can be used to calculate the AM flux of voltage.

$$\begin{cases} V_s = \dfrac{d\Phi_s}{dt} + R_s i_s \\ V_r = \dfrac{d\Phi_r}{dt} + R_r i_r \end{cases} \quad (9)$$

with: $V_s = V_{s\alpha} + jV_{s\alpha}, i_s = i_{s\alpha} + ji_{s\alpha}, i_r = i_{r\alpha} + ji_{r\alpha}, \Phi_s = \Phi_{s\alpha} + j\Phi_{s\alpha}, \Phi_r = \Phi_{r\alpha} + j\Phi_{r\alpha}$

From Equation (9), the flux expression can be extracted according to Equation (10).

$$\frac{d\Phi_s}{dt} = -R_s i_s + V_s \quad (10)$$

Equation (10) becomes as follows [45]:

$$\Phi_s = \int_0^t (-R_s i_s + V_s)dt \quad (11)$$

$$\Phi_s = V_s T_e + \Phi_{s0} - \int_0^t R_s\, i_s dt \quad (12)$$

Where, Φ_{s0} is the flux value in t = 0 s.

The flux can be calculated from the inverter operating pulses according to Equation (13). This flux is related to the DC voltage value [46].

$$\Phi_s(t) = \frac{2(S_1 + aS_2 + a^2 S_3)}{3} V_{dc} + \Phi_{s0} - \int_0^t R_s\, i_s dt \quad (13)$$

Equation (14) shows the expression stator flux modulus used in this work. The angle of the flux is neglected to determine the sectors, and to calculate it, Equation (15) is used. Equation (16) expresses the stator current of the AM.

$$|\Phi_s| = \sqrt{(\Phi_{s\beta}^2 + \Phi_{s\alpha}^2)} \quad (14)$$

$$\alpha_s = arctg \frac{\Phi_{s\beta}}{\Phi_{s\alpha}} \quad (15)$$

$$i_s = ji_\beta + i_\alpha \quad (16)$$

The current expressions in the αβ axis are included in Equation (17) [46].

$$\begin{cases} i_\alpha = \sqrt{\dfrac{2}{3}}\, i_{s\alpha} \\ i_{s\beta} = \dfrac{1}{\sqrt{2}}(-i_{sc} + i_{sb}) \end{cases} \quad (17)$$

To estimate the torque, the flux must be estimated first, and Equation (18) is used for this purpose. Estimating torque is related to measuring current, as the more accurate the current value is, the better the results.

$$T_e = 1.5 \times p(-\Phi_{s\beta}.I_{s\alpha} + \Phi_{s\alpha}.I_{s\beta}) \quad (18)$$

Despite the many advantages of this algorithm, such as rapid dynamic response, it gives unsatisfactory results in the event of a malfunction in the system, such as a change in machine parameters. Using this algorithm does not significantly reduce torque and current ripples. Also, this approach provides a higher THD value for the current which is not desirable. In the next section, a simple and effective solution is designed to overcome the problems and disadvantages of the 12 sectors DTC of the AM, mentioning the disadvantages and advantages of the proposed solution.

4. 12 Sector NN-DTC Algorithm

The 12-sector NN-DTC algorithm is the solution designed in this work to defeat the problems of the 12-sector DTC algorithm of AM. This algorithm relies on the use of NNs to enhance performance and robustness. NNs were adopted as a suitable solution due to the results obtained in the works [47-49].

This algorithm was relied upon for its ease of use, high robustness, and no need for an MM of the machine, which gives it greater efficiency if the AM parameters change, and a fast dynamic response. Therefore, the algorithm proposed in this section is a modification of the traditional algorithm, where ST and HC were dispensed with and replaced with a NN regulator, as shown in Figure 4. A neural regulator is used with three inputs: torque lines, sectors, and flux lines. Also, this regulator has three outputs which are pulses to operate the machine's inverter (Sa, Sb, and Sc).

The 12-NDTC algorithm is based on estimating torque, flux, and sectors. To estimate these values, both voltage and current are measured. Therefore, it is necessary to use measuring devices with high accuracy to minimize the error between the reference value and the measured value. In this approach, the estimation equations are the same as those mentioned in Section 3 of this paper. In this work, the training data source for the proposed NN-based DTC algorithm was taken from the traditional 12 sectors DTC approach, where the algorithm was trained and tested using data from the traditional 12 sectors DTC approach.

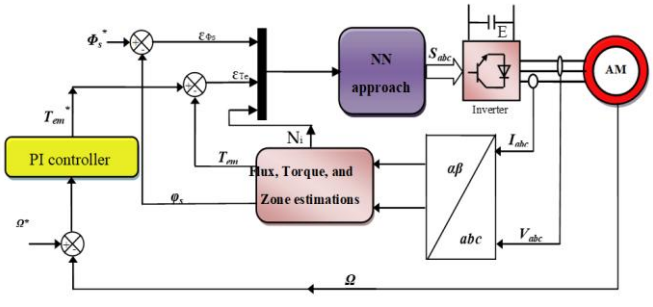

Fig. 4. 12 sectors NN-DTC algorithm of AM.

The 12-NDTC algorithm is based on the use of a PI-type regulator to control and change the speed, and it is the same controller used in the traditional 12-DTC algorithm listed in the third section. The gain values of this regulator were calculated using the method of simulation and experimentation, where values were taken that gave satisfactory results in terms of the value of THD of current and torque ripples.

Figure 5 represents the neural regulator used to control the operation of the AM inverter. The Levenberg–Marquardt (LM) algorithm was relied upon to obtain this neural regulator. The LM algorithm is known as the damped least squares approach, as it is used to solve nonlinear least squares problems. Using this algorithm allows for high performance and great efficiency. A neural algorithm of the type Gradient Descent with Momentum & Adaptive Learning Rate Backpropagation was used to embody the neural controller. This type is characterized by distinctive and effective performance. Also, it can be applied without having to know the MM of the AM. Table 3 represents the characteristics of the neural regulator used to improve the efficacy and competence of the 12-DTC algorithm of AM.

Figure 6 represents training for the neural controller. It is noted from Figure 6 that at 1000 epoch we obtain the best value for training performance, which is estimated at 0.027372. Figure 7 represents the internal structure of a neural regulator used to overcome the disadvantages of the 12-DTC strategy.

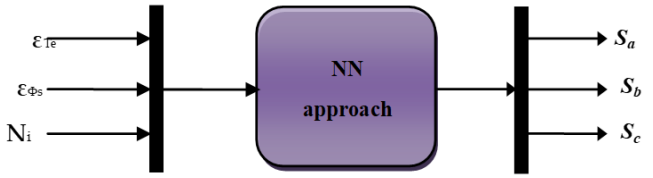

Fig. 5. Neural controller.

Table 3. Characteristics of the NN technique used.

Parameters	Value
Number of hidden layers	2
Number of neurons in first hidden layer	25
Learning rate	0.05
Display step (error display interval)	60 iterations
Number of input layers	1
Number of iterations (epochs)	1000
Number of output layers	1
Number of neurons in the input layer	3
Momentum coefficient (mc)	0.8
Number of neurons in the output layer	12
Error (goal)	0.005
Activation functions	Linear (output)

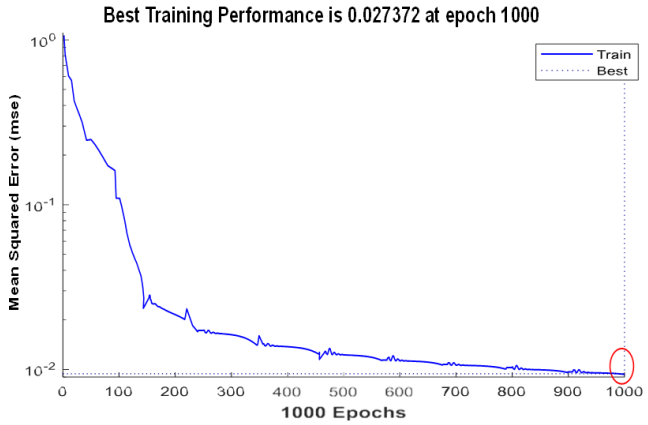

Fig. 6. Training.

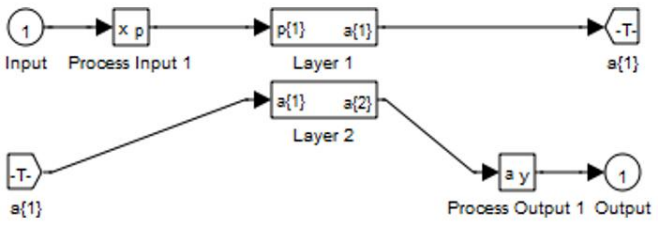

(a)

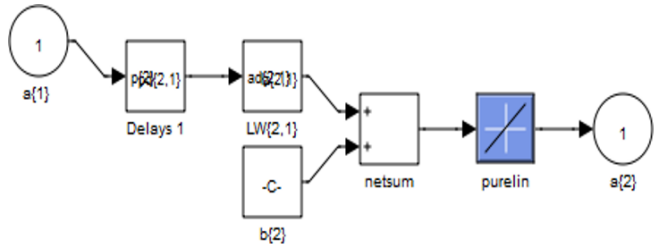

(b)

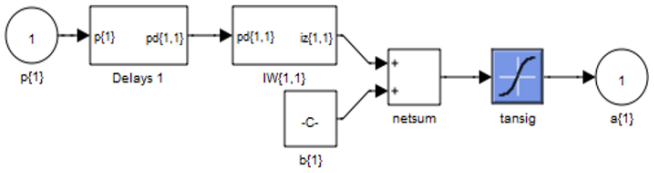

(c)

Fig. 7. Internal structure of a neural controller: (a) NN, (b) layer 1, (c) layer 2.

In Table 4, a comparison is made between the proposed 12-NDTC algorithm and the traditional DTC algorithm. The similarities and differences between the two algorithms are mentioned in this table. This table gives a clear picture of the proposed algorithm in terms of structure and its effectiveness, as the results of the fourth section were used to fill out this table.

The use of the 12-NDTC algorithm allows for a reduction in torque fluctuations and the THD of current compared to the 6-DTC, as confirmed in the next section. In the next section, a simulation of the designed algorithm is performed using several different tests.

Table 4. Similarities and differences between two algorithms.

Features	Traditional DTC algorithm	12 sectors DTC technique	Designed 12 sectors NN-DTC algorithm
ST	Yes	Yes	No
THD	High	Medium	Low
PI regulator of speed	Yes	Yes	Yes
Flux estimation	Yes	Yes	Yes
Torque estimation	Yes	Yes	Yes
Response dynamic	Fast	Fast	Very fast
NN controller	No	No	Yes
Robustness	Low	Medium	High
Number of sectors	6	12	12
Concordia transform	Yes	Yes	Yes
Flux/torque ripples	High	Medium	Low
Affected if machine parameters change	Great impact	Great impact	Little impact.

Although the replacement of hysteresis comparators and switching tables with NN method or intelligent networks has been explored previously, the present work introduces a distinct conceptual and technical framework within the 12-sector DTC paradigm. Specifically, the proposed method employs a unified neural decision structure that jointly determines the optimal voltage vector by considering both torque and flux sector information, rather than treating them as independent processes. Furthermore, NNs are considered a strategy that does not require knowledge of the mathematical model of the system under study, which ensures robustness in the face of parameter changes and load disturbances. This is fundamentally different from current 12-sector DTC approaches, including the method mentioned in [9], which rely on fixed control parameters and do not take advantage of online adaptation or integrated optimization for torque and flux control. Using this strategy requires a thorough understanding of the mathematical modeling of the system under consideration, making the proposed approach susceptible to changes in machine parameters. Furthermore, the proposed framework was validated through immediate implementation, demonstrating improved torque ripple suppression and dynamic response while reducing computational costs. These features together represent the most significant innovations in the proposed approach, surpassing previous improvements in the 12-sector DTC.

In Table 5, the approach designed in this paper is compared with the approach listed in Reference [9]. From this table, it is observed that the work done in this paper is completely different from the strategy designed in the work done in Reference [9] in terms of principle, type of controller used, performance, effectiveness, simplicity, etc.

Table 5. Comparison of the designed approach with the work done in reference [9].

Features	Proposed work in [9]	Suggested technique
Conceptual novelty	Enhancement within existing DTC structure	Reformulation of DTC decision process as an intelligent optimization problem using adaptive neural inference
Learning /Adaptation	Fixed control parameters; no adaptive learning	Adaptive neural network with self-adjusting weights that responds to changes in parameters/load
Core control strategy	12-sector DTC with Backstepping speed controller and P-MRAS stator resistance identification	12-sector DTC using unified neural decision structure replacing hysteresis comparators and tables
Torque and flux estimations	Yes	Yes
Integration of torque & flux control	Treated independently in the switching decision process	Joint optimization of torque and flux within a single neural decision framework
Robustness	High	High
Torque ripple reduction	Moderate improvement compared to classical DTC	Significant reduction due to adaptive neural control and finer voltage vector selection
Real-time implementation	Simulation and limited experimental validation	Fully validated in real-time embedded system implementation
Dynamic response	Improved using Backstepping control	Faster transient response through continuous, data-driven decision mapping
Complexity	High	Moderate

Table 5 therefore, illustrates the difference between the designer's work in this paper and the work completed in reference [9], summarizing the most important technical and conceptual differences. As demonstrated, the proposed controller offers a unified neural architecture capable of making real-time adaptive decisions, whereas current studies (such as [9]) rely on fixed control laws or offline-trained models. This integration of learning capabilities within a twelve-segment DTC framework is the key novel feature of this work.

5. Results

This section implements the algorithm proposed in this work using MATLAB. The results obtained are compared with the traditional 6-sector approach using a 3.5 kW AM. A comparison is made between the two strategies in terms of tracking references, reducing torque and flux fluctuations, and the value of the THD of the current. The AM parameters used in the simulation are as follows: f= 0.00325 Nm/rad/s, J= 0.043 kg·m², L_m= 0.267 H, L_s= 0.336 H, L_r= 0.2036 H, R_r= 1.88 Ω, R_s= 4.28 Ω, Φ_s=0.83 Wb, p = 2, n_r = 1480 rpm, P_n=3.5 kW, Te_n= 20 N·m, I_n= 11.1/6.5 A, V_n= 230/400 V, and f_s= 50 Hz.

5.1. Test 1: No-load Start-up and Steady-state Operation

In the first test, the motor is operated at a constant speed of 1000 rpm without applying any load. The results of this test are represented in Figure 8. Figure 8a illustrates the torque for the two algorithms. This torque reaches a value of 20 N.m in the case of startup and then gradually decreases until it reaches a value of 0 N.m when the speed is equal to the value of 1000 rpm. It is also noted that the 6-DTC algorithm significantly reduced torque ripples compared to the 6-DTC algorithm.

Figure 8b represents the speed of the two algorithms. This speed initially changes gradually until it reaches the reference value estimated at 1000, after which it remains constant. It is noted that the designed algorithm provided a faster response time than the DTC technique, which indicates the effectiveness and efficiency of this algorithm.

Figure 8c represents the current for the algorithms used in this work. This current has a sinusoidal shape for the two algorithms with ripples. The proposed algorithm gave the high quality of the current compared to the DTC algorithm, which shows its high performance and the extent of its ability to enhance the quality of the current.

Figure 8d represents the trajectory of the stator flux components Φisd and Φisq for the two algorithms. This is a circular trajectory for both controls with ripples. The proposed algorithm gave a better trajectory than the DTC technique in terms of ripples.

Figure 8e represents the position of the flux vector Φs for the two controls. It is noted that the two algorithms have the same value as the position of the flux vector Φs. This position takes the shape of saw teeth. Figure 8f represents the THD value if the two algorithms are used.

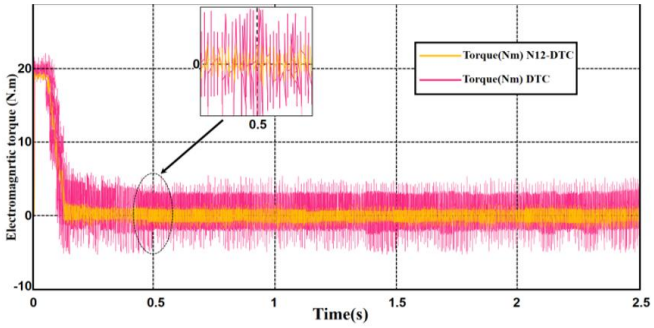

(a) Torque

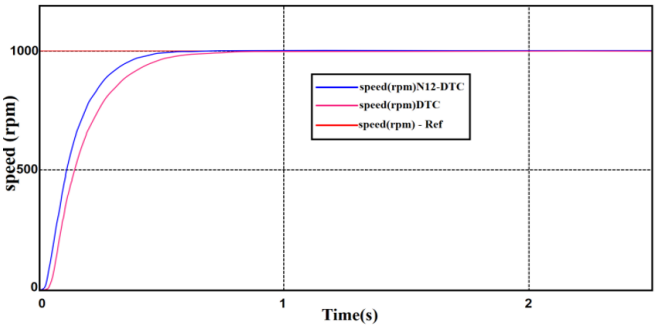

(b) Speed

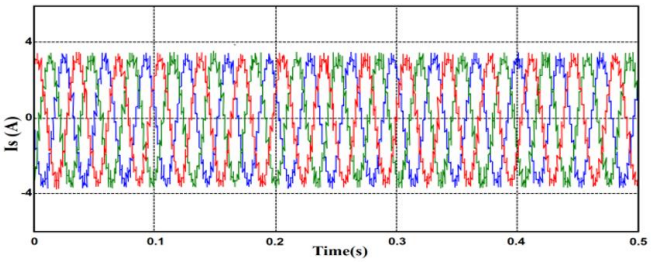

(c.1) Current: DTC

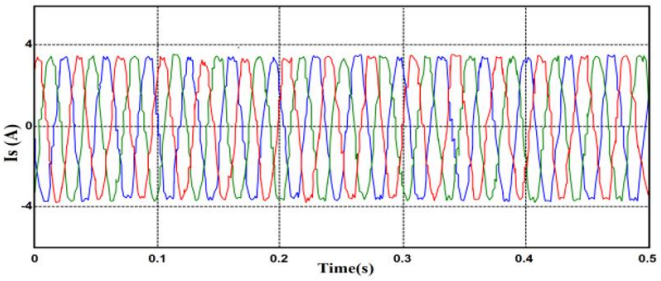

(c.2) Current: 12 sectors neural DTC

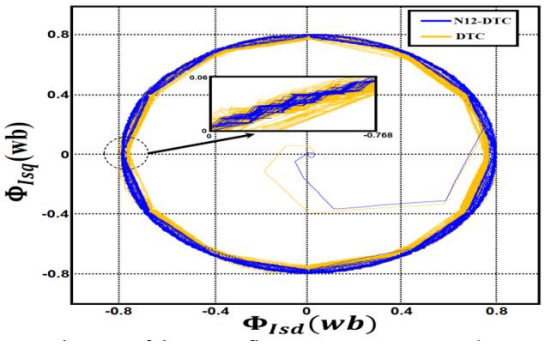

(d) Trajectory of the stator flux components Φi_{sd} and Φi_{sq}

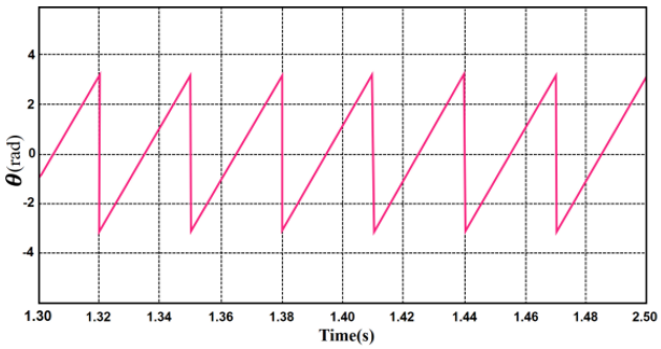

(e.1) Position of the flux vector Φs: DTC

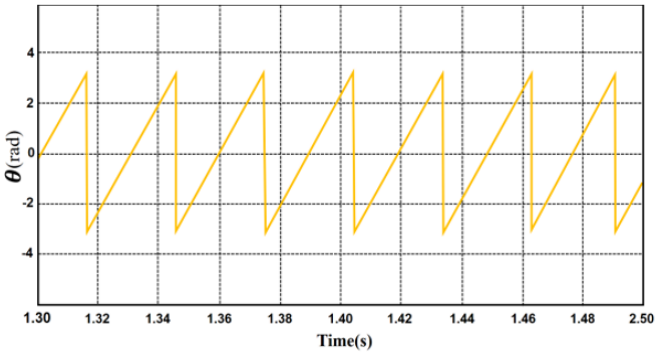

(e.2) Position of the flux vector Φs: 12 sectors neural DTC

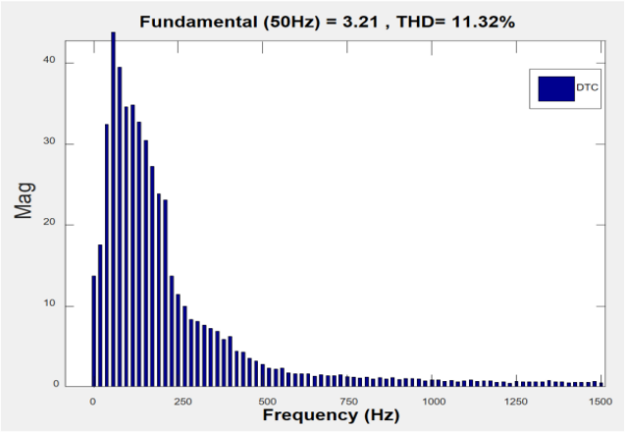

(f.1) THD of current: DTC

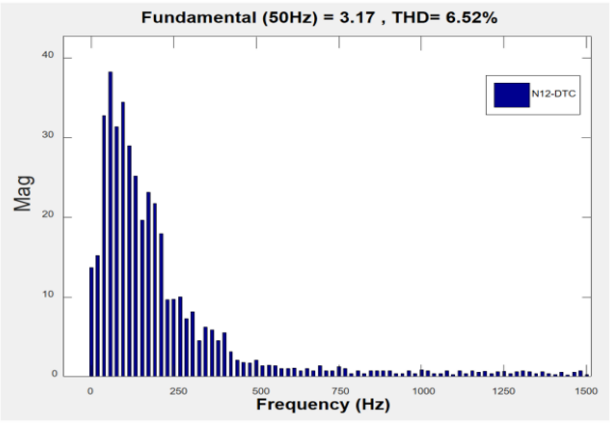

(f.2) THD of current: 12 sectors neural DTC

Fig. 8. Results of the first test.

According to the two figures in Figure 8f, the THD value was 11.32 % and 6.52 % for DTC and 12-NDTC, respectively. Therefore, the proposed algorithm significantly minimized the THD value, as this minimization was estimated at 42.40 % compared to the DTC technique. On the other hand, it is noted that the amplitude value of the fundamental signal (50 Hz) for the two controls was estimated at 3.21 A and 3.17 A for the traditional approach and the 12-sector neural DTC strategy, respectively. These values indicate that the conventional 6 sectors DTC approach has an advantage in amplitude value compared to the 12-sector neural DTC approach. Therefore, the amplitude value of the approach designed in this test can be considered negative, as this disadvantage can be attributed to the characteristics of the neural approach used. This disadvantage can be overcome in the future by adding other strategies integrated with the neural controller.

Table 6 presents the numerical results of the first test of the two approaches. This table presents the values and reduction ratios for torque/flux ripples and velocity/flux response time. This table shows that the designed approach yielded significantly better numerical results than the conventional 6 sectors DTC technique. From Table 6, the designed approach reduced the torque, flux, and current ripples by 55 %, 55 %, and 74.81 %, respectively, compared to the conventional 6 sectors' DTC strategy. On the other hand, the designed 12 sectors' neural DTC technique yielded significantly better times for both velocity and flux than the conventional 6 sectors' DTC strategy, with ratios of 43.91 % and 39 %, respectively. These ratios demonstrate the effectiveness of the designed 12 sectors' neural DTC approach in improving the properties of the studied system.

Table 6. Numerical results of the first test.

Performance metric	Traditional technique	Proposed technique	Ratios (%)
Torque ripples (Nm)	4.50	2.0	55
Speed response time (ms)	230	129	43.91
Flux ripples (Wb)	0.045	0.020	55
Flux response time (ms)	140	85	39
Current ripples (A)	0.393	0.099	74.81

5.2. Test 2: Speed Variation Under No-load Conditions

In this test, the 12-NDTC technique is studied in the case of changing the speed from 1000 rpm to 1500 rpm while no load is applied. The results of this test are listed in Figure 9.

Figure 9a represents the speed change as a function of time for the two algorithms. The speed follows the reference for the two algorithms, with the proposed algorithm having an

advantage in terms of response time compared to the 6 sectors DTC algorithm.

Figure 9b represents the torque change for the two algorithms. This torque is affected by a change in speed at the moment t = 1 s, where an increase in the value of the torque is observed until it reaches a value of 20 N·m, then it gradually decreases to a value of 0 N·m with the presence of ripples. The torque ripples are much lower when using the proposed algorithm compared to the DTC technique.

Figure 9c represents the current for the two algorithms. This current is affected by the change in the speed of the machine, as its value increases at t = 1s. The current remains sinusoidal for both algorithms. Also, the designed algorithm gave high quality for this current compared to the DTC.

Figure 9d represents the trajectory of the stator flux components Φi_{sd} and Φi_{sq} for the two controls. This flux trajectory remains circular, with the proposed algorithm having an advantage in terms of ripples compared to the DTC technique, and the results of the previous test are the same.

These results highlight the superiority of the 12-NDTC technique and its competence in reducing flux ripples, current, and torque. In this test, it is noted that the position of the flux vector Φs remains the same shape as in the previous test for the two controls (Figure 9e).

The THD of current value for the two algorithms is represented in Figure 9f. This value was 7.46 % and 14.25 % for the designed algorithm and DTC technique, respectively. So, the proposed algorithm provided a better value for THD compared to the DTC technique. The proposed algorithm reduced the THD value by an estimated 47.65 %.

It is also noted that the amplitude values of the fundamental signal (50 Hz) were estimated to be 2.95 A and 3.23 A for both the conventional approach and the 12-sector neural DTC technique, respectively. These values demonstrate that the amplitude value is better in the case of using the designed approach compared to the conventional 6 sectors DTC approach, where the amplitude value was improved by a percentage of 8.67 %. This percentage indicates that the quality of the current is very high if the designed algorithm is used, which is a good thing.

Table 7 presents the numerical results of the second test of the two controllers. This table clearly demonstrates the superiority of the designed approach over the conventional 6 sectors DTC approach in terms of reducing torque/current ripples and improving the response time to velocity and flux. From this table, the designed 12 sectors neural DTC technique reduces the torque, flux, and current ripples by 54 %, 54 %, and 68.43 %, respectively, compared to the conventional approach.

On the other hand, the designed approach reduced the response time to speed and flux by 44 % and 39.46 % compared to the traditional 6 sectors DTC technique. These figures demonstrate the effectiveness of the designed 12 sectors neural DTC technique in this test and its high ability to improve the properties of the studied system, making it a promising solution.

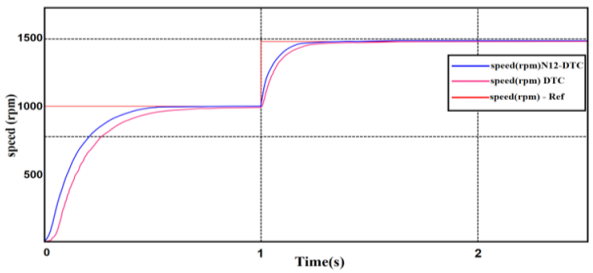

(a) Speed

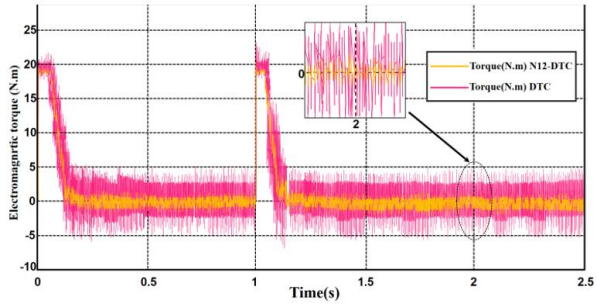

(b) Torque

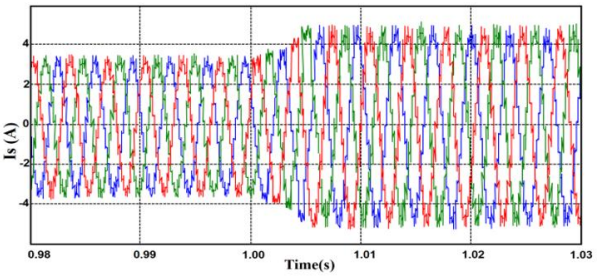

(c.1) Current: DTC

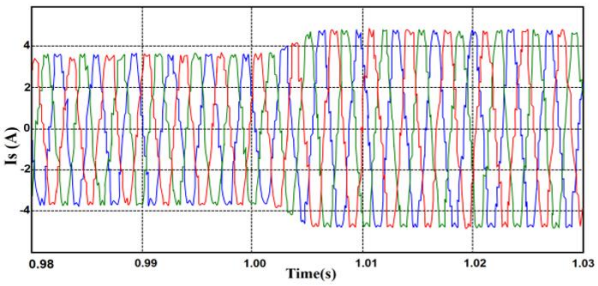

(c.2) Current: 12 sectors neural DTC

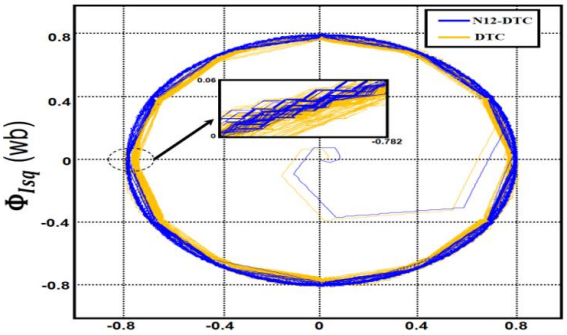

(d) Trajectory of the stator flux components Φi_{sd} and Φi_{sq}

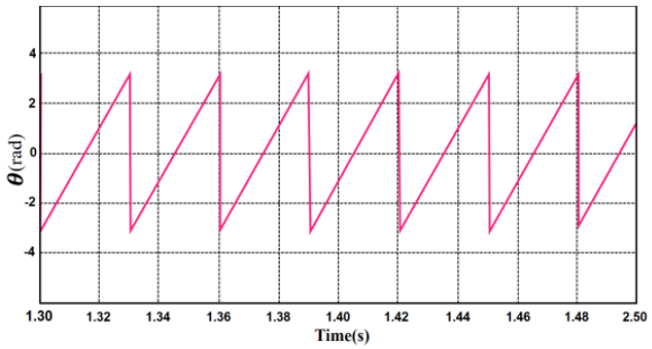

(e.1) Position of the flux vector Φs: DTC

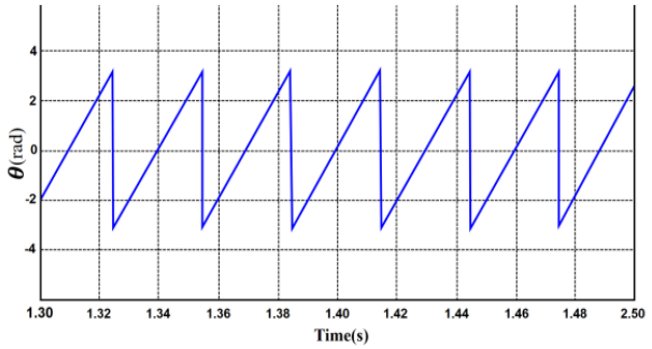

(e.2) Position of the flux vector Φs: 12 sectors neural DTC

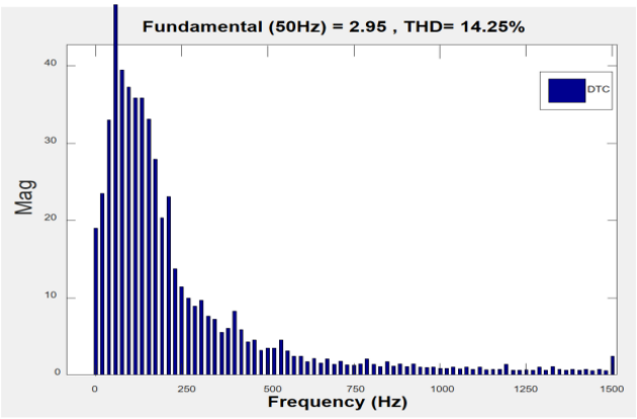

(f.1) THD of current: DTC

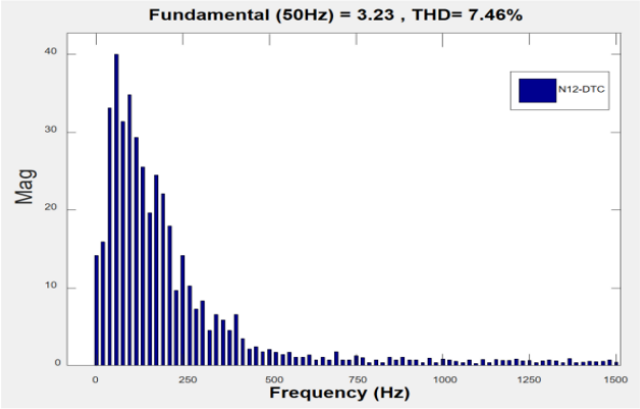

(f.2) THD of current: 12 sectors neural DTC

Fig. 9. Results of the second test.

Table 7. Numerical results of the second test.

Performance metric	Traditional technique	Proposed technique	Ratios (%)
Torque ripples (Nm)	5.00	2.3	54
Speed response time (ms)	330	185	44
Flux ripples (Wb)	0.050	0.023	54
Flux response time (ms)	147	89	39.46
Current ripples (A)	1.036	0.327	68.43

5.3. Test 3: Test with Resistive Torque (Load Condition)

This test is different from previous tests. In this test, the speed is fixed at 1000 rpm, and the load (10 N·m) is applied in the time range from 1 to 2 s. The results of this test are listed in Figure 10.

Figure 10a represents the torque change as a function of time. This torque follows the reference well while having a quick dynamic response. It is noted that there are fluctuations at the level of this torque, and these fluctuations are less when using the proposed algorithm compared to the 6 sectors DTC technique.

Figure 10b represents the speed change for the two algorithms as a function of time. First, the speed changes gradually until it reaches the reference value, with the proposed algorithm having an advantage in terms of response time compared to the DTC technique. After that, the speed remains constant and follows the reference value well, with an exceedance of the limit value at the time points of 1 s and 2 s as a result of the torque change.

Figure 10c represents the current for the two algorithms. This current is affected at the moment of 1s, where its value is observed to increase, and this is a result of applying a load at this moment. This current remains sinusoidal for both algorithms, with the proposed algorithm having an advantage in terms of current quality compared to 6 sectors DTC technique. In this test, the trajectory of the stator flux components Φi_{sd} and Φi_{sq} remains circular (Figure 10d), with the proposed algorithm having an advantage in terms of undulations compared to the 6 sectors DTC technique, which produces the same results as the previous two tests. These results highlight the advantage of the designed algorithm and its high efficiency.

Figure 10e represents the position of the flux vector Φs in this test for the two controls. This position remains the same as in the previous tests, as it is not affected by changes in speed, load torque, or machine parameters.

Figure 10f represents the THD of the current for the two algorithms in the third test. This value was 16.76 % and 10.13

% for the DTC technique and the proposed approach, respectively. The proposed algorithm significantly minimized the THD value compared to the 6 sectors DTC technique, which highlights that the current quality is high if the proposed algorithm is used. This reduction in THD value was estimated at 39.56 %. On the other hand, it is noted that the amplitude value of the fundamental signal (50 Hz) was equal to 3.32 A for the traditional 6 sectors DTC approach and 3.28 A for the proposed approach. Therefore, the amplitude value is higher in the case of using the conventional DTC approach compared to the designed approach. Therefore, this amplitude value can be considered a disadvantage of the designed approach in this test. This disadvantage can be attributed to the number of neurons and the number of internal layers, which can be overcome in the future by using other strategies, such as the NARX algorithm.

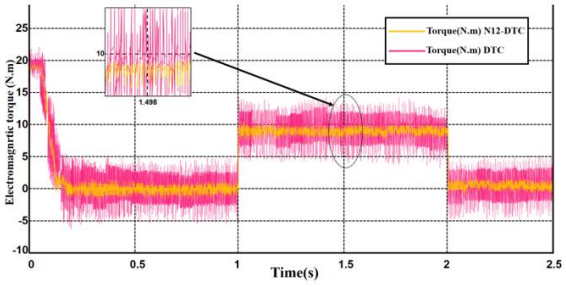

(a) Torque

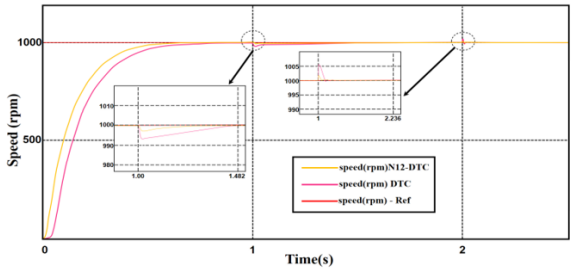

(b) Speed

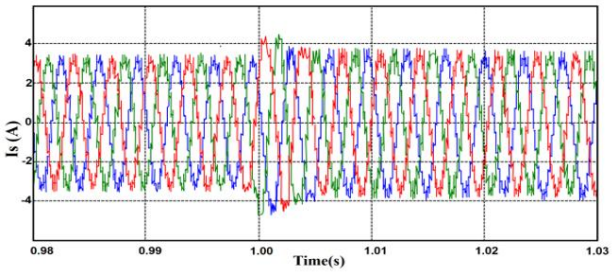

(c.1) Current: DTC

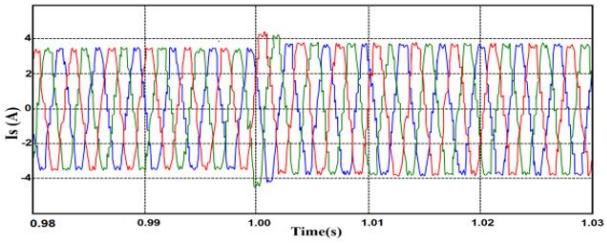

(c.2) Current: 12 sectors neural DTC

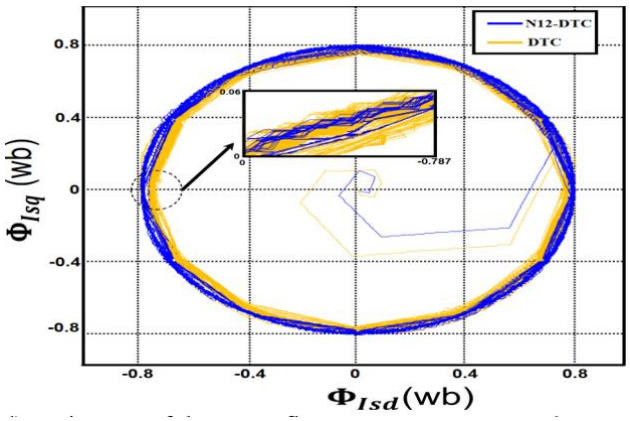

(d) Trajectory of the stator flux components Φi_{sd} and Φi_{sq}

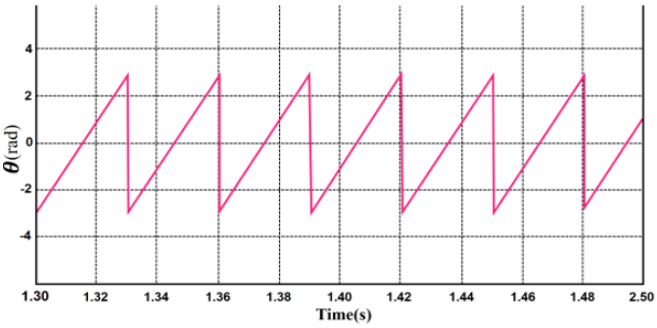

(e.1) Position of the flux vector Φs: DTC

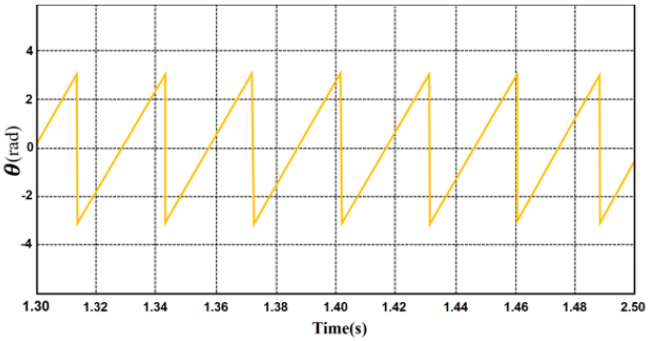

(e.2) Position of the flux vector Φs: 12 sectors neural DTC

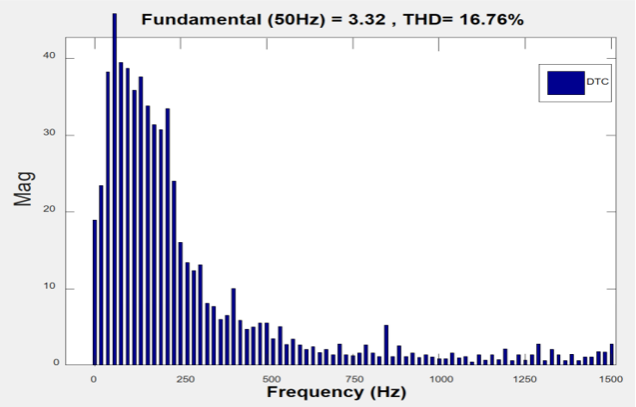

(f.1) THD of current: DTC

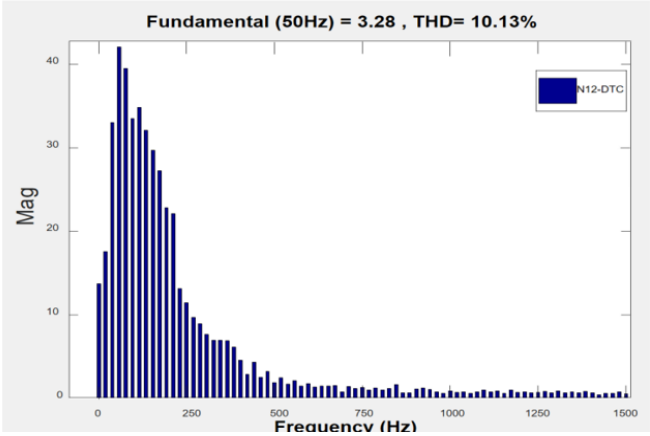

(f.2) THD of current: 12 sectors neural DTC

Fig. 10. Results of the third test.

Table 8 presents the numerical results of the third test of the two techniques. This table gives the values and reduction ratios for the torque, flux, and current ripples. It also gives the reduction ratios and response time values for the flux and velocity. From this table, it is observed that the proposed 12 sectors' neural DTC strategy gave better values than the conventional approach. Table 8 shows that the designed 12 sectors neural DTC approach reduced the torque, current, and flux ripples by 54.39 %, 66.12 %, and 62.32 %, respectively, compared to the conventional approach. Furthermore, the designed 12 sectors neural DTC technique reduced the response time to flux and speed by 40.96 % and 49.52 %, respectively, compared to the conventional 6 sectors DTC approach. These results demonstrate the effectiveness of the designed approach in this test and its high performance in improving the current/torque quality and dynamic speed/flux response. These results make the designed 12 sectors' neural DTC approach attractive for other industrial applications.

Table 8. Numerical results of the third test.

Performance metric	Traditional technique	Proposed technique	Ratios (%)
Torque ripples (Nm)	5.70	2.6	54.39
Speed response time (ms)	420	212	49.52
Flux ripples (Wb)	0.069	0.026	62.32
Flux response time (ms)	166	98	40.96
Current ripples (A)	1.684	0.469	66.12

5.4. Test 4: Robustness Test

This test is completely different from the previous tests. This test examines the effectiveness and efficiency of the designed approach under the condition of changing machine parameters. In this test, the machine parameters are modified so that the resistance values are multiplied by 2 and the inductance values are multiplied by 0.5. Furthermore, the speed is held at 1000 rpm with no load applied.

The purpose of this test is to study the impact of the designed approach on machine parameter changes compared to the conventional 6 sectors' DTC approach. The graphical results of this test are shown in Figure 11. Figure 11a represents the speed changes for two controls. Despite the machine parameter changes, the speeds for both controls closely follow the reference value, with the designed approach having an advantage in response time over the conventional 6 sectors' DTC technique. Figure 11b represents the torque variation for the two controls as machine parameters change. This figure shows that the torque is affected by machine parameter changes, as this change is evident in the height of the ripples. However, the designed approach produced significantly lower ripples than the conventional approach, demonstrating the effectiveness of the designed approach and its insensitivity to machine parameter changes compared to the conventional approach.

Figure 11c represents the change in current as the machine parameters change. This figure demonstrates that the current is affected by the change in machine parameters for the two controls, as evidenced by the presence of ripples. Despite the change in machine parameters, this current remains sinusoidal. Figure 11c demonstrates that the current quality is higher when using the proposed approach compared to the traditional 6 sectors DTC technique, proving that the designed approach is less affected by machine parameter changes. Figure 11d represents the trajectory of the stator flux components FISD and FISC using both controls. Despite the parameter changes, the trajectory of the stator flux components remains circular, similar to the observations in the previous tests. However, ripples are observed, and these ripples are significantly lower in the designed technique compared to the traditional 6 sectors DTC technique. Figure 11e represents the change in the position of the flux vector for the two controls as the machine parameters change. From this figure, it is noted that despite the change in the machine parameters, the change in the position of the flux vector for the two controls remains the same as in the previous tests, proving that the position of the flux vector for the two controls is not affected by changes in the AM parameters.

Figure 11f represents the THD of current for two controls under the condition of changing machine parameters. From this figure, it is noted that the THD value was estimated at 14.06 % for the traditional 6 sectors DTC strategy and 7.98 % for the proposed approach. These values highlight the superiority of the proposed approach over the traditional approach, as the THD value was reduced by approximately 43.24% compared to the traditional 6 sectors DTC approach. On the other hand, Figure 11f shows that the amplitude value of the fundamental signal (50 Hz) was estimated to be 3.28 A and 3.29 A for both the conventional and proposed approaches, respectively. Therefore, the proposed 12 sectors neural DTC strategy gave a better amplitude value compared to the conventional approach, which highlights the effectiveness and efficiency of this designed approach in improving the current quality despite the change in the machine parameters compared to the conventional approach.

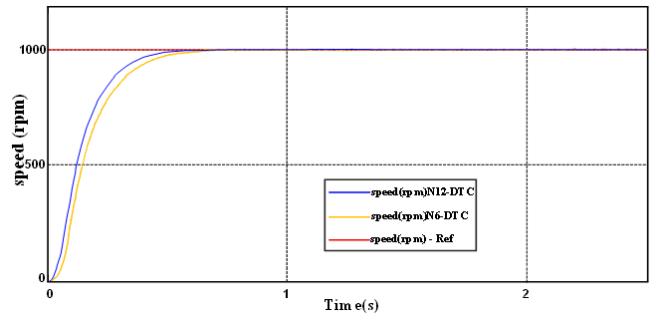

(a) Speed

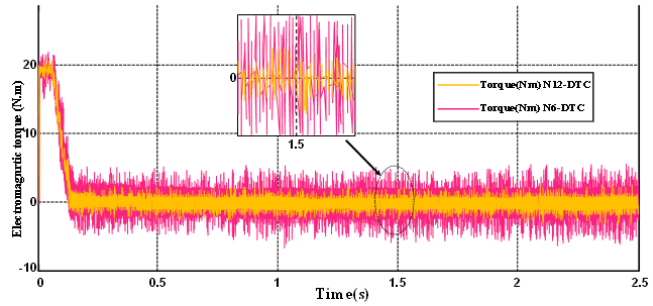

(b) Torque

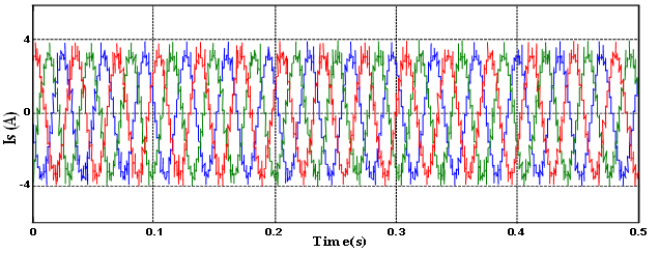

(c.1) Current: DTC

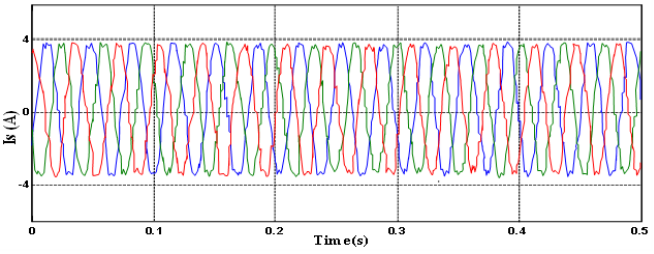

(c.2) Current: 12 sectors neural DTC

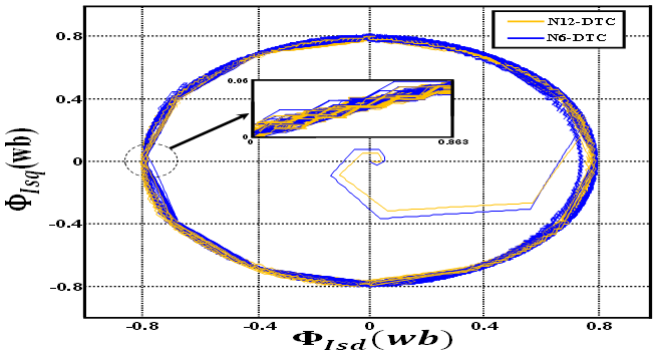

(d) Trajectory of the stator flux components Φi_{sd} and Φi_{sq}

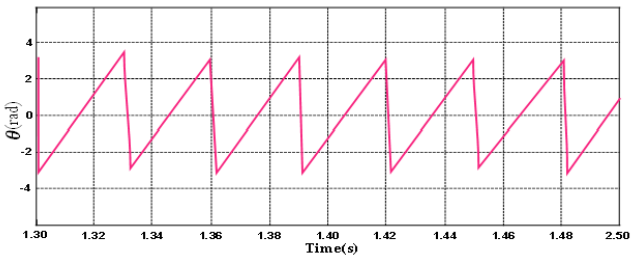

(e.1) Position of the flux vector Φs: DTC

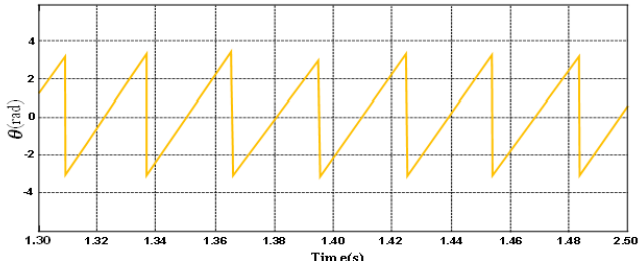

(e.2) Position of the flux vector Φs: 12 sectors neural DTC

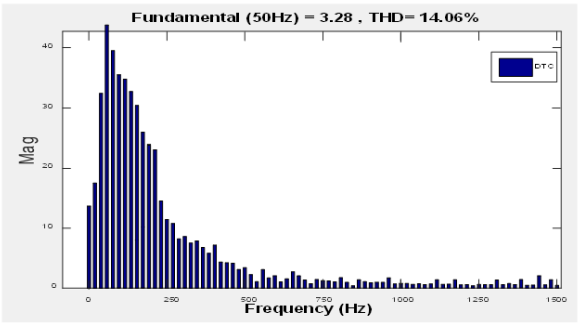

(f.1) THD of current: DTC

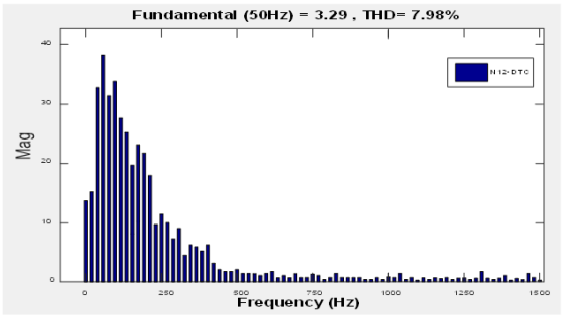

(f.2) THD of current: 12 sectors neural DTC

Fig. 11. Results of the fourth test.

Table 9 presents the numerical results of the fourth test of the two controllers. Table 9 shows that the proposed 12 sectors neural DTC approach yielded very satisfactory results compared to the conventional 6 sectors DTC approach in terms of current, torque, and flux ripples. Table 9 also demonstrates the effectiveness of the proposed 12 sectors neural DTC approach in improving the response time to velocity and flux compared to the conventional 6 sectors DTC technique. The proposed 12 sectors neural DTC technique reduced the torque, flux, and current ripple values by 54.15 %, 59.32 %, and 48.32 %, respectively, compared to the

conventional 6 sectors DTC strategy. Furthermore, the proposed approach reduced the response time to velocity and flow by 30.45 % and 42.31 %, respectively, compared to the conventional 6 sectors DTC approach. These ratios demonstrate the effectiveness, efficiency, and high performance of the proposed 12 sectors neural DTC technique compared to the conventional 6 sectors DTC approach, making it a promising solution for future control applications.

Table 10 represents a study of the extent to which the values of current THD and amplitude of the fundamental signal (50 Hz) were affected between tests using both controls. Table 10 shows that the THD value changed across tests for both controls. Therefore, it can be said that the THD value is affected by both load and speed changes. Using the 6 sectors DTC approach, the THD value changed by 20.56 % between Test 2 and Test 1 and by 32.46 % between Test 1 and Test 3. In the case of the proposed 12 sectors neural DTC approach, the THD value changed by 12.60 % between Test 1 and Test 3 and by 35.64 % between Test 3 and Test 1. These ratios indicate that the proposed 12-sector NN-DTC approach had a lower impact on the THD value between Test 2 and Test 1 compared to the traditional approach. However, between Test 3 and Test 1, the proposed 12-sector neural DTC had a greater impact compared to the 6 sectors DTC. On the other hand, the amplitude value of the fundamental signal (50 Hz) was significantly affected in the two control tests. Table 10 shows that the value of the amplitude changed between the first and second tests by a percentage of -7.85 % and +1.86 % for the traditional and proposed approaches, respectively. Therefore, the value of the amplitude decreased when the 6 sectors DTC was used, but its value increased when the proposed 12-sector neural DTC approach was used. Furthermore, in the third test, the amplitude value increased significantly compared to the first test for both controls. This increase was estimated at 3.31 % and 3.35 % for the 6-DTC and proposed approaches, respectively. Therefore, the 12-sector NN-DTC provided a greater amplitude effect between the third test and test 1, demonstrating the effectiveness and efficiency of the proposed designed 12-sector NN-DTC in improving the fundamental signal (50 Hz) amplitude value compared to the 6-DTC. Table 10 also shows that the THD of current increased in the fourth test compared to the first test for both controls. This increase can be attributed to the change in the machine parameters in the fourth test. The difference in THD between the fourth and first tests was estimated to be +2.74 % and +1.46 % for the classical and designed approaches, respectively. Therefore, the proposed approach produced a lower THD difference than the conventional approach, demonstrating its effectiveness despite the change in AM parameters. Also, the value of the fundamental signal (50 Hz) amplitude increased significantly in the fourth test compared to the first test, which shows that the value of this amplitude was affected by changing the machine parameters for the two controls. The difference in amplitude between the fourth and first tests was estimated at +0.07 A and +0.12 A for the conventional and proposed approaches, respectively. Therefore, the proposed 12 sectors neural DTC approach yielded a larger difference compared to the conventional approach, highlighting the effectiveness of the proposed 12 sectors neural DTC in improving the amplitude value despite the change in the machine parameters.

Table 9. Numerical results of the fourth test.

Performance metric	**Traditional technique**	**Proposed technique**	**Ratios (%)**
Torque ripples (Nm)	5.89	2.7	54.15
Speed response time (ms)	289	201	30.45
Flux ripples (Wb)	0.059	0.024	59.32
Flux response time (ms)	156	90	42.31
Current ripples (A)	0.896	0.463	48.32

Table 10. Study the extent to which the values of the fundamental signal (50 Hz) amplitude and current THD are affected in the case of using the two controls.

Current THD and amplitude of fundamental signal (50 Hz)		Traditional DTC technique	12 sectors neural DTC
Amplitude of fundamental signal (50 Hz)	Test 1	3.21	3.17
	Test 2	2.95	3.23
	Test 3	3.32	3.28
	Test 4	3.28	3.29
	Test 2 – Test 1	-0.26	+0.06
	Test 3 – Test 1	+0.11	+0.11
	Test 4 – Test 1	+0.07	+0.12
	(Test 2 – Test 1)/ Test 2	-7.85%	+1.86%
	(Test 3 – Test 1)/ Test 3	3.31%	+3.35%
	(Test 4 – Test 1)/ Test 4	+2.13%	+3.65%
Current THD (%)	Test 1	11.32	6.52
	Test 2	14.25	7.46
	Test 3	16.76	10.13
	Test 4	14.06	7.98
	Test 2 – Test 1	+2.93	+0.94
	Test 3 – Test 1	+5.44	+3.61
	Test 4 – Test 1	+2.74	+1.46
	(Test 2 – Test 1)/ Test 2	+20.56%	+12.60%
	(Test 3 – Test 1)/ Test 3	+32.46%	+35.64%
	(Test 4 – Test 1)/ Test 4	+19.49%	+18.30%

6. Empirical Results

In this part, the experimental implementation of the designed algorithm is discussed, comparing the results obtained with the 6-DTC technique. The experimental work of the designed algorithm was designed using the experimental setup shown in Figure 12. This experimental work differs from several previously completed experimental works such as [19, 29].

In experimental work, the computational burden is a major factor and is taken into consideration in the case of industrial applications. Requests for lower arithmetic regulators with better competence, and performance are always high. Therefore, the 12-NDTC technique is most suitable for industrial applications. In this experimental work, real tools were used to implement it, as a permanent magnet synchronous motor with a power of 3.5 kW and a load of 5.5 kW was used. In this experimental work, a two-level inverter was used to feed the machine. The experimentally completed inverter consists of an array of IGBT-type transistors.

The experimental work consists of two main sections, as shown in Figure 12. These two sections are the control part, which expresses the elements related to control, such as the proposed algorithm, and the second section is the power section, which consists of several elements, such as the AM machine.

In this experimental work, we relied on a control panel dSPACE 1104 for generating PWM control signals with TTL 0/5 V logic. Use a control panel dSPACE is based on the use of MATLAB, where the 12-NDTC technique is realized in MATLAB and is linked between MATLAB and the dSPACE control panel.

Using MATLAB/Simulink real-time applications are easy to program in Simulink using specific blocks of the real-time interface (RTI) toolbox, which allows the inputs and outputs of the dSPACE DS1104 board to be configured. ControlDesk is the second program used in this experimental work, which is used to load the program code onto the board (written graphically in Simulink, compiled, and converted to C code). It also enables real-time monitoring of measured or calculated data using graphical or digital displays. The Texas Instrument DSP (Digital signal processor) type TMS320F240 is used to handle additional processing tasks.

In this experimental work, information exchange between components and experimental work parts is managed via an external connector board (CP1104/dSPACE), connected to the board through a shielded cable. This board facilitates the reception of analog signals through BNC connectors. Also, it adapts the signal to PWM control signals and possible error signals from the Semikron converter. The use of this board allows the integration of different measuring sensors into the experimental setup.

The signal conditioning interface converts between 0/5 V TTL logic and 0/15 V CMOS logic. This conversion is critical as the DS1104 control board operates with 0/5 V TTL signals, while the inverter requires 0/15 V CMOS signals.

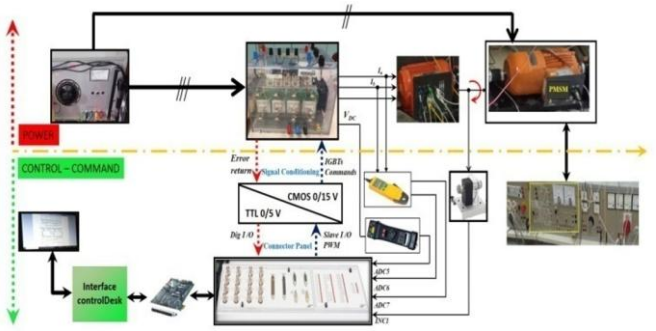

Fig. 12. Schematic diagram of the experimental platform.

To measure current, closed-loop Hall effect current sensors LEM LA55TP are used, and to measure voltage, closed-loop Hall effect voltage sensors LEM LV100-500 are used. Also, an incremental encoder is used to measure the motor speed. In this experimental work, a protection filter with a cut-off frequency of about 500 Hz (well above the fundamental frequency of 50 Hz) was used between each sensor and the analog-to-digital converter.

Figure 13 represents the experimental work performed for the proposed algorithm. This figure gives a clear picture of the various parts used and composing the experimental work.

Three different tests are proposed to experimentally verify the efficacy and efficiency of the 12-NDTC technique. Also, the competence of the 12-NDTC technique is compared with the 6-sector DTC algorithm. Experimentally, the same machine parameters used in the simulation section are used.

6.1. Test 1: No-Load Startup and Steady-State Operation

In this test, a torque scale was used: 5 V and a gain of 0.1, and for flux a gain of 1 and a gain of 2 V was used. The reference speed is fixed at 1000 rpm. The results of this test are represented in Figure 14. Figure 14a represents the experimentally obtained torque and speed for the two controls. The torque follows the reference well and is the same thing for speed. It is noted that the designed algorithm gave fewer undulations than the 6 sectors DTC technique and a faster dynamic response to speed compared to the 6 sectors DTC technique.

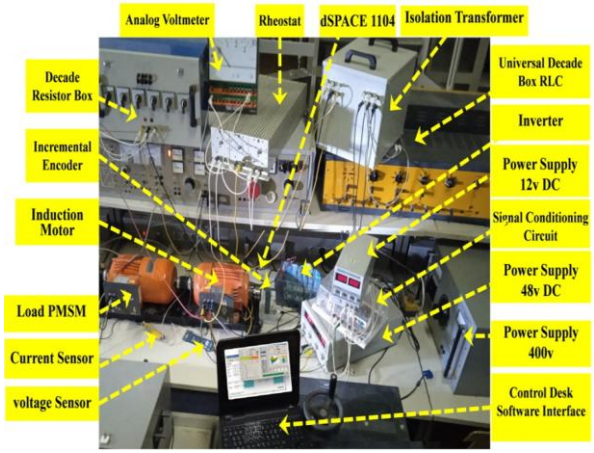

Fig. 13. Experimental prototype setup.

Figure 14b represents zoom-in rotor speed. This figure shows that using the proposed algorithm increases the dynamic speed performance compared to using the 6 sectors DTC technique. Also, it is noted that the speed response time was 212 ms and 400 ms for both the 12-NDTC strategy and the DTC technique. Therefore, the 12-NDTC technique significantly reduced the response time compared to the 6 sectors DTC technique. This reduction was estimated at 47 % compared to the 6 sectors DTC technique, as this percentage highlights the strength and competence of the designed algorithm and its ability to improve dynamic response.

Figure 14c shows a zoom representation of the stator currents (1 div = 5 A) for the two algorithms. These currents are absorbed by the motor, and it is noted that these currents have a sinusoidal shape with ripples. These fluctuations are low when using the 12-NDTC strategy compared to DTC technique.

Figure 14d represents the change of both the stator flux and its components as a function of time for the three control methods. It is noted that the flux takes a constant value and follows the reference well (1 div = 0.2 Wb). The flux fluctuations are low when using the designed algorithm compared to the 6 sectors DTC technique (see Figure 13e). Also, the flux components take a sinusoidal shape with distortions. These distortions are less in the proposed algorithm compared to the 6 sectors DTC technique.

Figure 14e represents zoom in both position and flux. The results listed in this figure are the same as the results listed in the simulation, where the position of stator flux takes the form of saw teeth.

Figure 14f represents the evolution of the flux components for the two algorithms. It is noted that the shape of the evolution of the flux components takes a circular shape, which is the same as the simulation results. Also, the proposed algorithm provided better development than traditional 6 sectors DTC technique in terms of ripples.

Figure 14g represents the THD of the current obtained from the experimental work of the two algorithms. This value was 12.83 % and 8.87 % for the 6 sectors DTC technique and the 12-NDTC strategy, respectively. Therefore, the designed algorithm minimized the value of THD experimentally compared to the 6 sectors DTC technique. This reduction was estimated at 30.87 %. This percentage proves that the algorithm has an effective performance in reducing current ripples and improving its quality compared to the 6 sectors DTC technique. Experimentally, it was observed that the amplitude of the fundamental signal (50 Hz) was 3.29 A for the conventional 6 sectors DTC technique and 3.22 A for the designed 12 sectors neural DTC approach. These results are almost the same as the simulation results in the first test. Therefore, the conventional 6 sectors DTC technique gave a better amplitude value than the designed 12 sectors neural DTC approach. Therefore, this amplitude can be considered a drawback of the designed approach in this test. This drawback can be overcome in the future by using a fractional-order control strategy or by changing the number of internal layers of the neural controller.

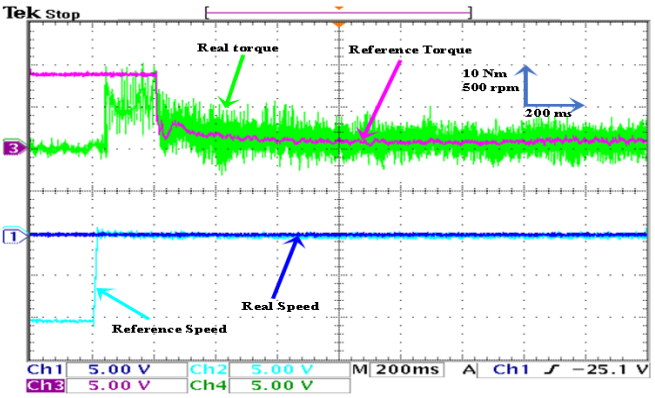

(a.1) Torque and speed (first empirical test): DTC

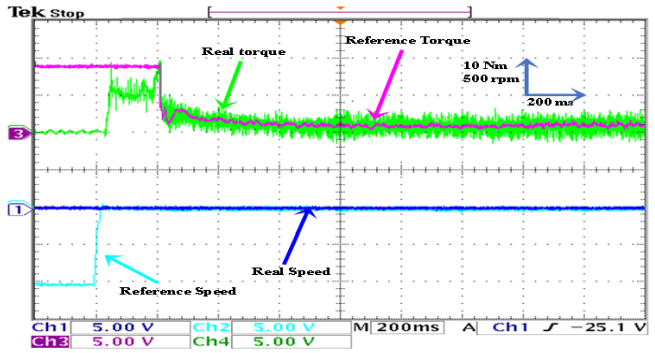

(a.2) Torque and speed (first empirical test): 12 sectors neural DTC

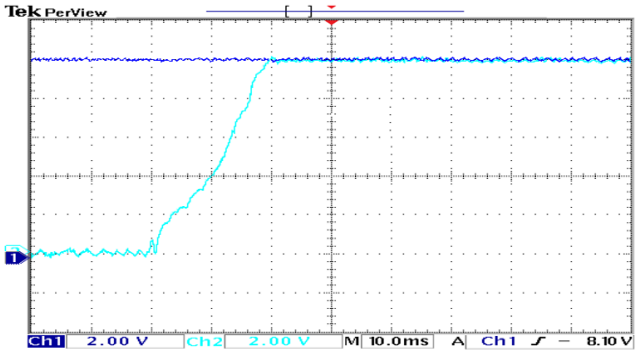

(b.1) Zoom on the rotor speed (first empirical test): DTC

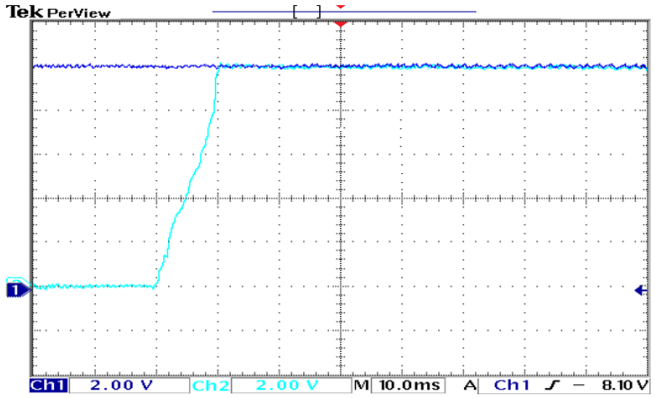

(b.2) Zoom on the rotor speed (first empirical test): 12 sectors neural DTC

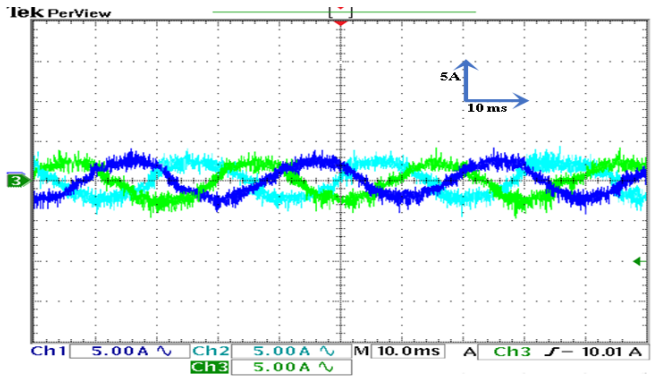

(c.1) Zoom in the currents (first empirical test): DTC

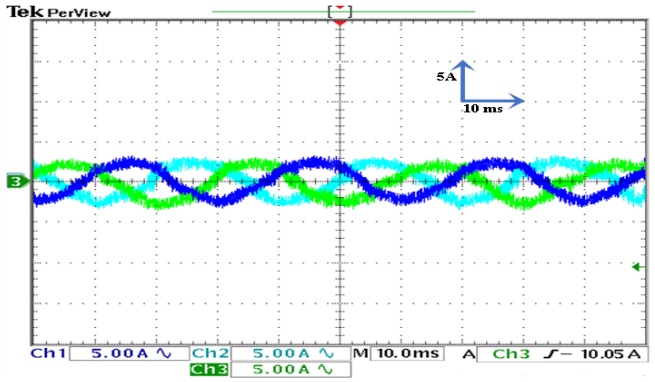

(c.2) Zoom in the currents (first empirical test): 12 sectors neural DTC

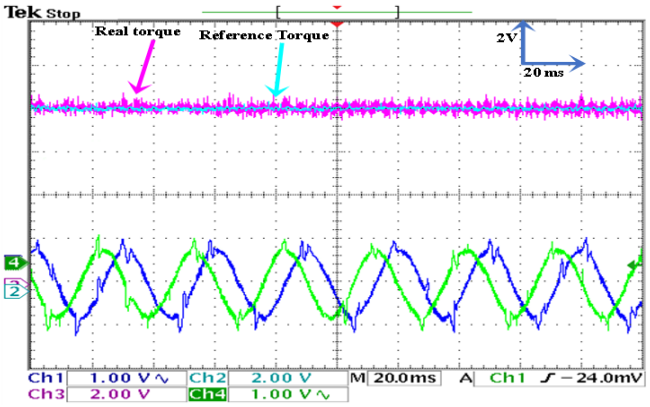

(d.1) Stator flux (first empirical test): DTC

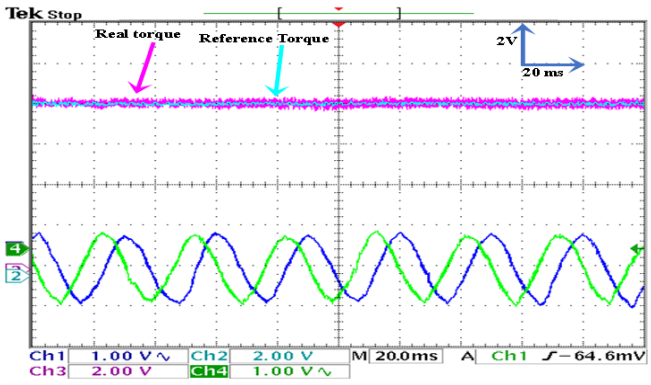

(d.2) Stator flux (first empirical test): 12 sectors neural DTC

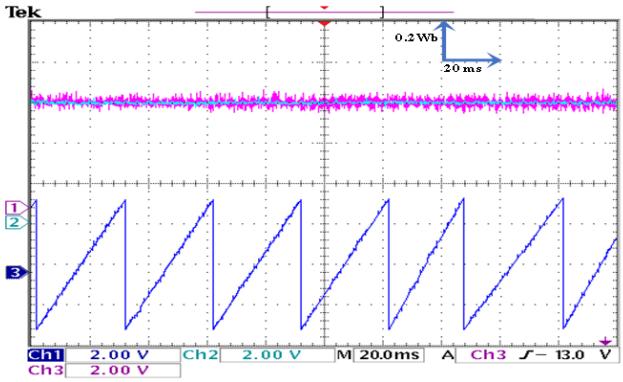

(e.1) Zoom in the stator flux and position (first empirical test): DTC

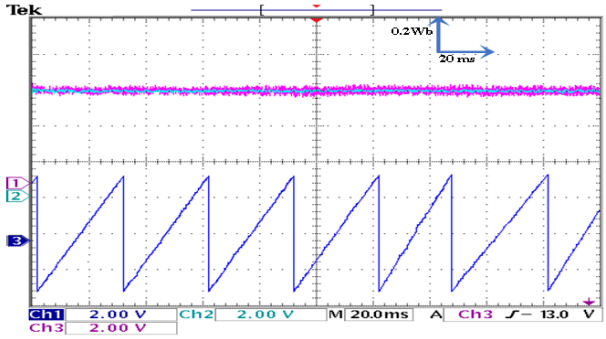

(e.2) Zoom in the stator flux and position (first empirical test): 12 sectors neural DTC

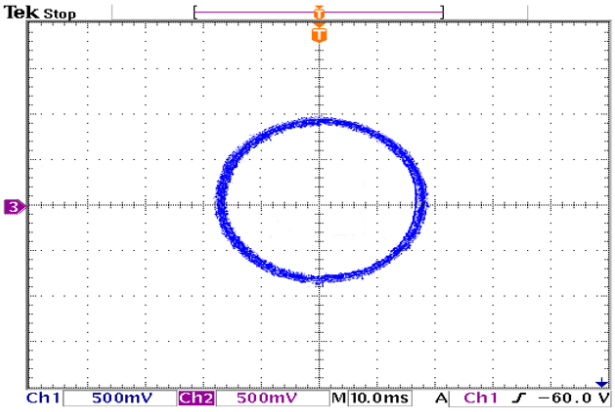

(f.1) Trajectory of the stator flux (first empirical test): DTC

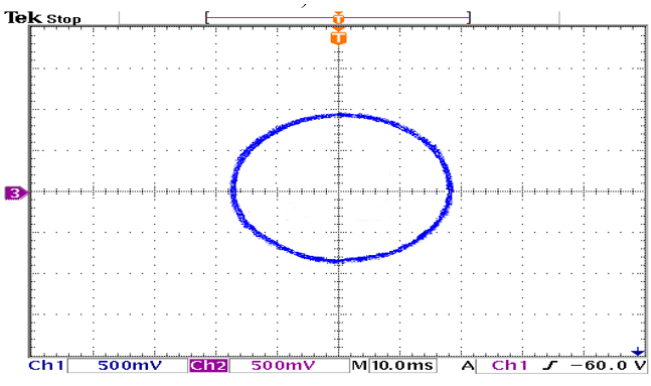

(f.2) Trajectory of the stator flux (first empirical test): 12 sectors neural DTC

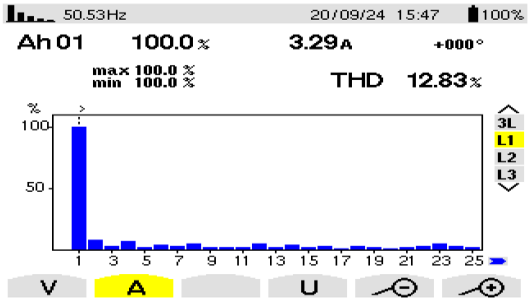

(g.1) THD of current (first empirical test): DTC

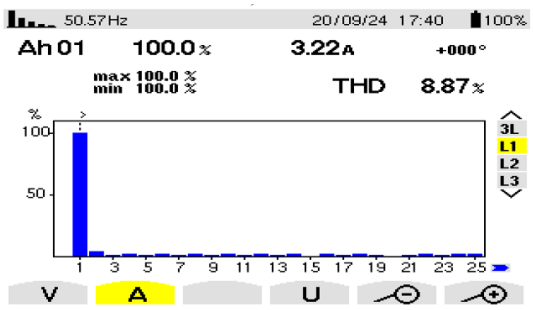

(g.2) THD of current (first empirical test): 12 sectors neural DTC

Fig. 14. Results of the first empirical test.

6.2. Test 2: Speed Variation

In this subsection, the 12-NDTC technique is tested in the case of changing rotational speed. The reference speed is changed from 1000 rpm to 1480 rpm under no-load conditions. The results of this test are represented in Figure 15. For this test, a 500 mV scale with a gain of 0.01 was used for torque measurements, a 500 mV scale with a gain of 0.0001 for speed measurements, and a 200 mV scale with a gain of 0.0001 for speed measurements. Gain of 0.1 for flux measurements.

Figure 15a represents the torque and motor speed of the two algorithms. The speed follows the reference well with some distortion. These distortions are non-existent in the proposed approach compared to the 6 sectors DTC technique. It is noted in this test that the designed algorithm provided a better dynamic response to rotational speed than the 6 sectors DTC technique. Also, the proposed algorithm minimized exceeding the limit value of rotation speed compared to the 6 sectors DTC technique.

When changing the rotation speed from 1000 rpm to 1480 rpm, it is noted that the torque value increased. Therefore, an increase in rotational speed corresponds to an increase in the torque value, after which the torque returns to its previous value as a result of the use of the PI regulator. From Figure 15a, it is noted that the designed algorithm reduced the value of torque ripples compared to the 6 sectors DTC technique.

Figure 15b represents the change in current for the two algorithms in Test 2. This current takes a sinusoidal shape, with an increase in the value of the current observed at the moment of the speed change, which is normal. Also, the proposed algorithm provided a high quality of current compared to the 6 sectors DTC technique.

Figure 15c represents the flux (1 div = 0.2 Wb) and its components (1 div = 1 Wb) at the value of 1480 rpm. From this figure, it is noted that the flux is affected by changing the value of the rotation speed, as it is observed that the limit value is exceeded. This overshoot was less severe when using the proposed algorithm compared to the 6 sectors DTC technique. Moreover, the designed algorithm minimized the value of flux ripples in this test compared to the 6 sectors DTC technique. The flux components are sinusoidal for the two controls, with the proposed algorithm having an advantage in terms of quality compared to the DTC technique.

Figure 15d represents the evolution of the flux components of the two algorithms. This development is the same as in the previous test and in the simulation. It is noted that the designed algorithm provided better development than the 6 sectors DTC technique in terms of quality.

The value of THD of the current is listed in Figure 15e. This value is estimated to be 19.09 % and 11.03 % for both the DTC technique and the proposed algorithm. Therefore, the designed algorithm minimized the THD value in this test compared to the 6 sectors DTC technique. This minimization was estimated at 42.22 %. On the other hand, Figure 15e shows that the amplitude of the fundamental (50 Hz) current signal was 3.29 A for both controls. Therefore, the amplitude values were the same for both controls. These results highlight the effectiveness of the designed approach in improving the characteristics of the current and the control system as a whole.

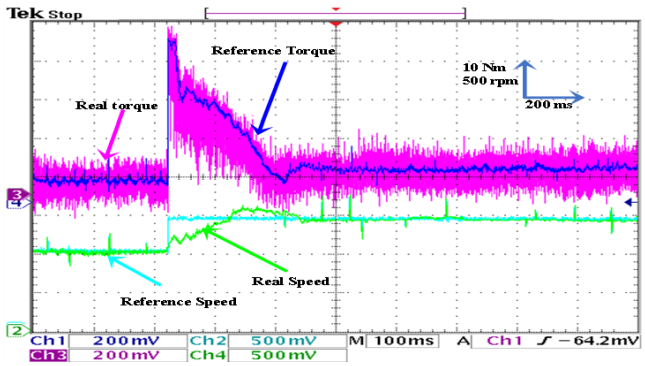

(a.1) Rotor speed and torque (experimental test 2): DTC

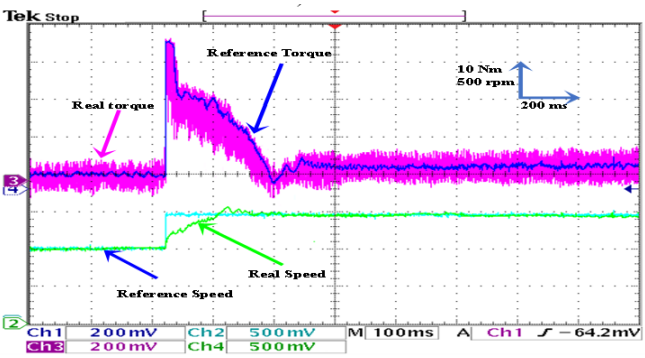

(a.2) Rotor speed and torque (experimental test 2): 12 sectors neural DTC

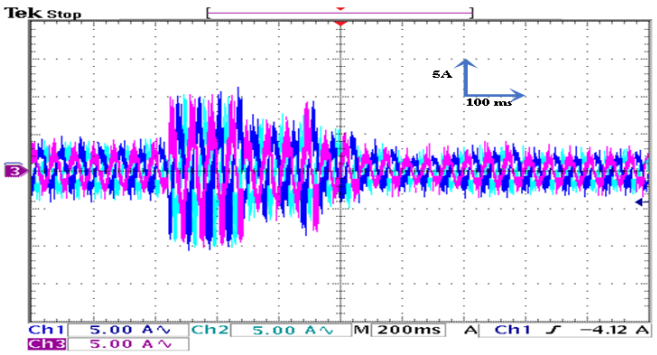

(b.1) Stator currents (experimental test 2): DTC

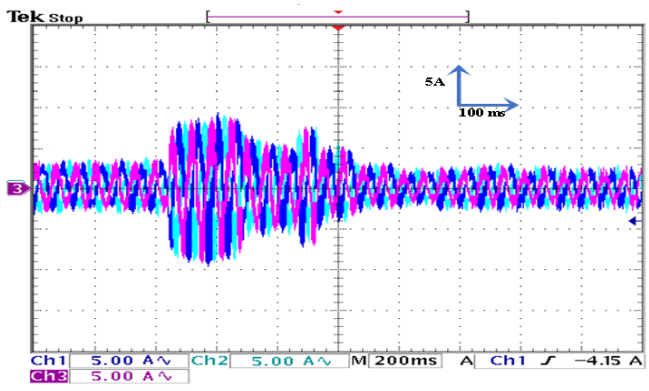

(b.2) Stator currents (experimental test 2): 12 sectors neural DTC

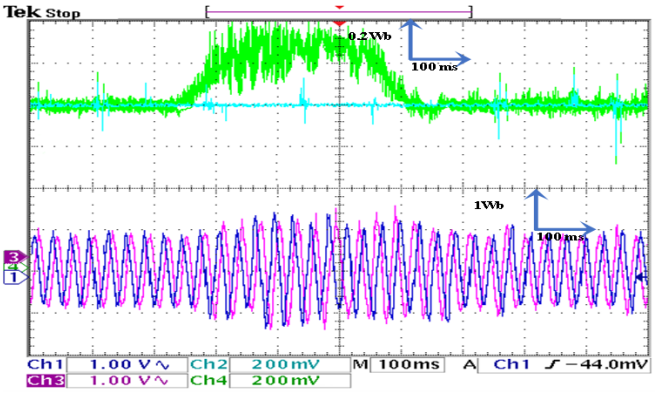

(c.1) Stator flux and its components for 1480 rpm (experimental test 2): DTC

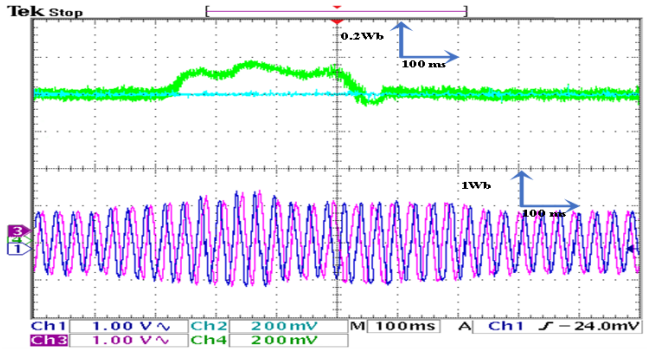

(c.2) Stator flux and its components for 1480 rpm (experimental test 2): 12 sectors neural DTC

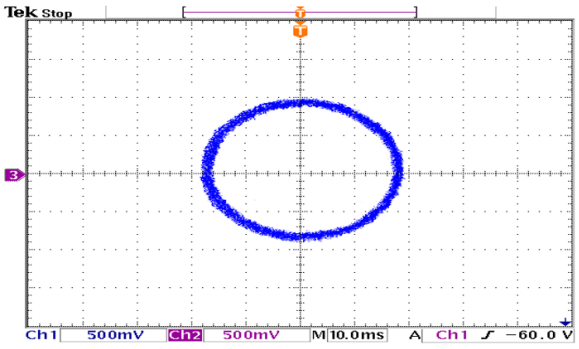

(d.1) Evolution of flux components (experimental test 2): DTC

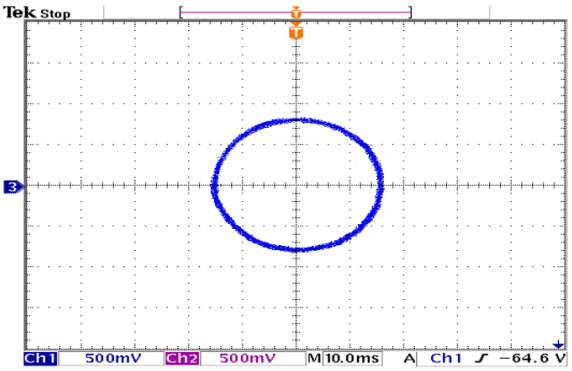

(d.2) Evolution of flux components (experimental test 2): 12 sectors neural DTC

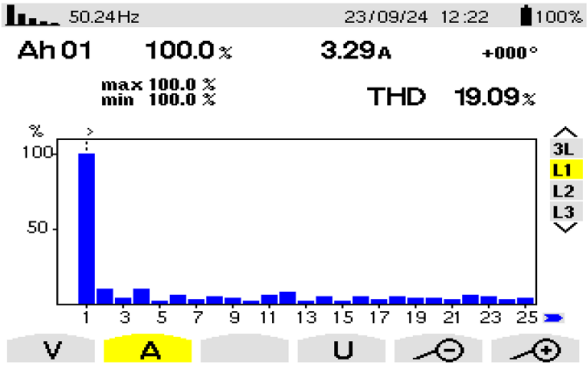

(e.1) THD of current (experimental test 2): DTC

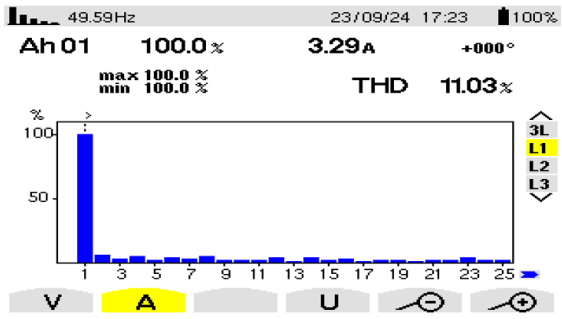

(e.2) THD of current (experimental test 2): 12 sectors neural DTC

Fig. 15. Results of the second empirical test.

6.3. Test 3: Load Test

This test differs from the previous two experimental tests. In this test, the speed is fixed at 1000 and a load is applied. The sampling time is set to $Te = 10^{-4}$ s using Euler's method. The reference static flux is 0.8 Wb. In this test, a 500 mV scale with a gain of 0.01 was used for torque measurements, and a 500 mV scale with a gain of 0.0001 was used for speed measurements. The results of the third pilot test are shown in Figure 16.

Figure 16a shows the torque (1 div = 5 N.m) and the current I_{sa} (1 div = 5 A) of the AM at the moment when the load is applied. It can be observed from this figure that the AM torque closely follows the reference torque for the three proposed algorithms. Additionally, the electrical current increases at the moment the load is applied, with this increase corresponding to the applied load (the value of the applied resistant torque). Furthermore, there are torque and current ripples, as shown in Figure 16b, which are more pronounced in the case of the 6 sectors DTC technique compared to the proposed algorithm. These applied results are consistent with those presented in the simulation section, indicating the validity of the previously presented results and the superiority of the 12-NDTC technique.

The AM speed and torque are illustrated in Figure 16c. From this figure, it is observed that the speed (1 div = 500 rpm) closely follows the reference for the proposed algorithm. The DTC technique and proposed algorithm experience overshoot, and their response times can be compared to the proposed algorithm when the load is applied. These results convincingly confirm the simulation results and demonstrate that the 12-NDTC technique is superior to both the 6 sectors DTC technique, particularly in terms of reducing torque fluctuations. The evolution of the flux components of the AM in this test is shown in Figure 16d for the two controls. The evolution of the flux components in this test remains the same as in the previous two tests with a circular shape. The proposed algorithm gave a much better shape for the evolution of flux components than the 6 sectors DTC technique.

In this test, the THD of the current value is listed in Figure 16e for the two algorithms. According to Figure 16e, the THD value experimentally was 23.93 % and 12.03 % for both the 6 sectors DTC technique and the designed algorithm, respectively. Therefore, the designed algorithm minimized the value of THD experimentally by an estimated percentage of 49.73 % compared to the 6 sectors DTC technique. Figure 16e shows that the fundamental (50 Hz) current amplitude was 3.19 A for the conventional 6 sectors DTC technique and 3.29 A for the designed approach. These values indicate that the amplitude is larger in the designed approach. The experimental amplitude value for the designed approach is almost the same as the amplitude obtained using simulation in the third test. These experimental results highlight the efficacy and strength of the 12-NDTC technique in improving the control system features and current quality compared to the 6 sectors DTC technique. Therefore, the proposed algorithm can be relied upon in the future in industrial applications such as propulsion and traction.

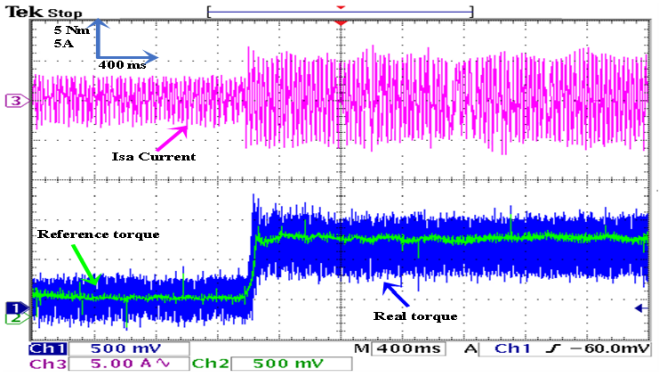

(a.1) Torque and stator current I_{sa} (experimental test 3): DTC

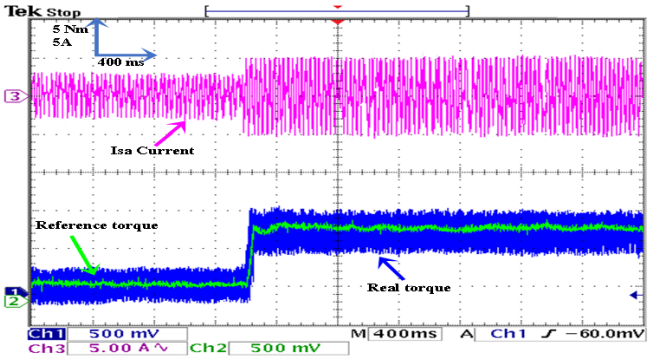

(a.2) Torque and stator current I_{sa} (experimental test 3): 12 sectors neural DTC

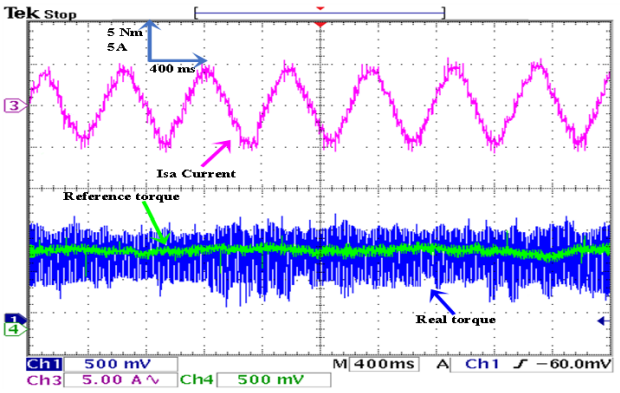

(b.1) Zoom in the torque and current (experimental test 3): DTC

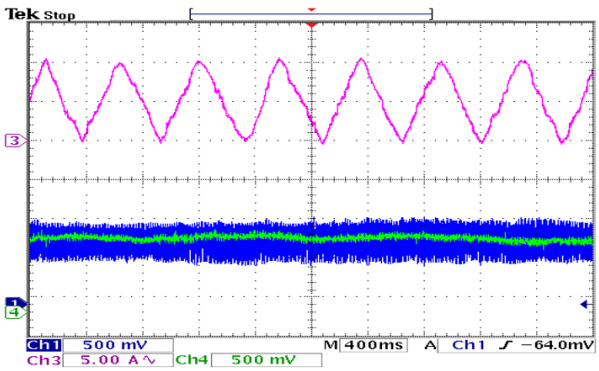

(b.2) Zoom in the torque and current (experimental test 3): 12 sectors neural DTC

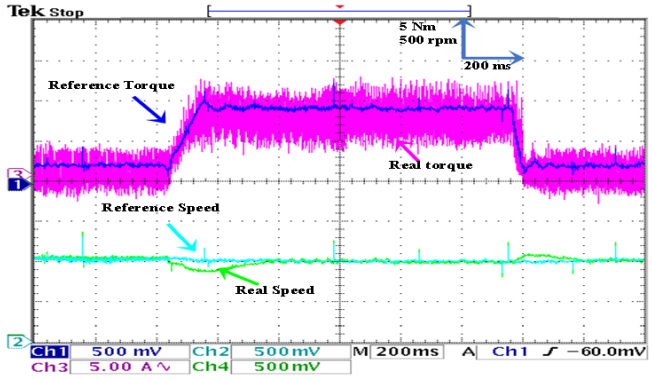

(c.1) Rotor speed and electromagnetic torque (experimental test 3): DTC

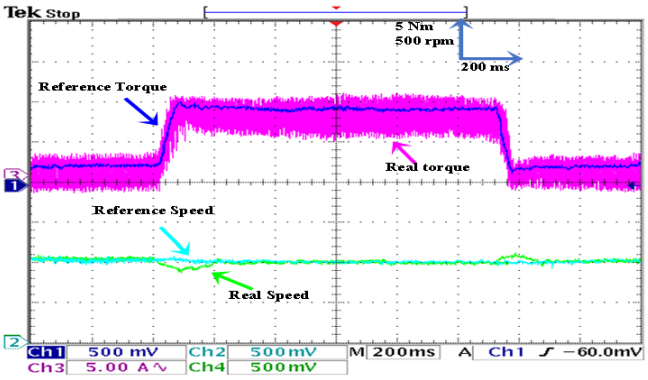

(c.2) Rotor speed and electromagnetic torque (experimental test 3): 12 sectors neural DTC

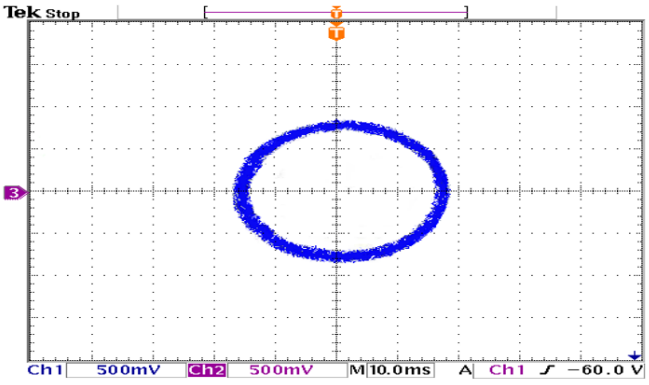

(d.1) Evolution of flux components (experimental test 3): DTC

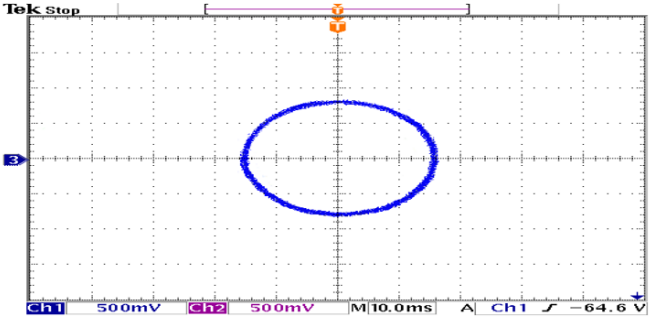

(d.2) Evolution of flux components (experimental test 3): 12 sectors neural DTC

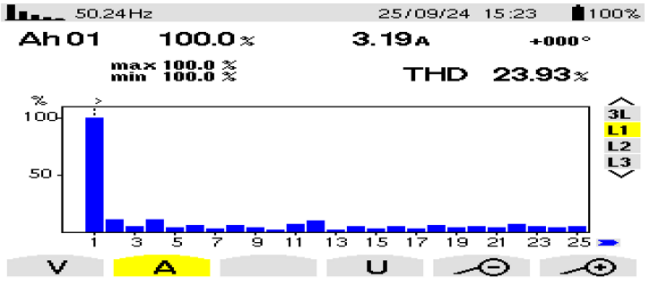

(e.1) THD of current (experimental test 3): DTC

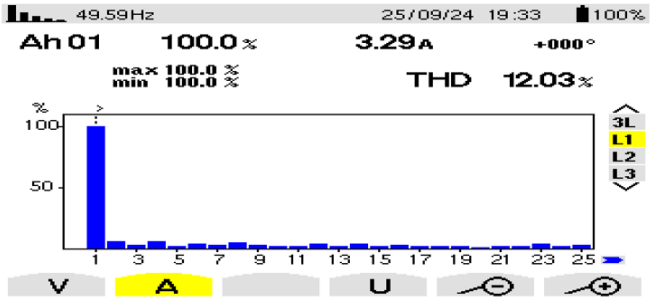

(e.2) THD of current (experimental test 3: 12 sectors neural DTC

Fig. 16. Results of the third empirical test.

6.4. Fourth Experimental Test: Low Speed Operation

This experimental test differs from previous experimental tests. In this test, the effectiveness of the designed 12 sectors neural DTC approach is studied at low speeds. The speed varies from 800 rpm to 250 rpm and then to 125 rpm, with the results shown in Figure 17.

According to Figures 17a and 17b, the speed of the two techniques follows the reference value well, with the designer approach having an advantage over the traditional 6 sectors DTC approach regarding response time (blue curve). Also, a threshold value is observed when using the traditional 6 sectors DTC approach, but the designed approach does not exceed the threshold value for speed, demonstrating the great capability and effectiveness of this approach.

The position of the flux vector for the two techniques is represented by the purple curve. It is noticeable that the shape of the position of the flux vector is a sawtooth signal as in the previous tests. From Figures 17a and 17b, it is observed that the period of the position of the flux vector signal varies with the change in rotational speed, where the period is lowest for a speed value equal to 800 rpm, and the lower the speed, the higher the period value. On the other hand, it is observed that the quality of the position of the flux vector signal is better in the case of using the proposed 12 sectors neural DTC strategy compared to the conventional 6 sectors DTC technique.

The current for the two controls is represented by the green curve. This current for the two controls remains sinusoidal with ripples. These ripples are lower in the designed 12 sectors neural DTC approach compared to the conventional 6 sectors approach.

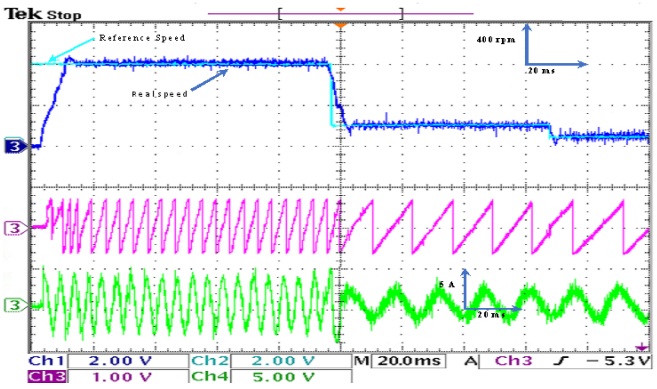

(a) DTC

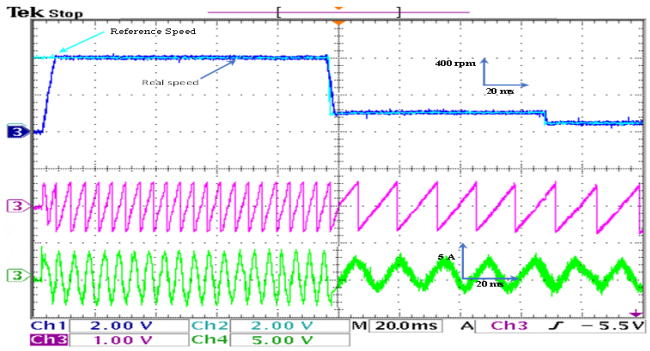

(b) 12 sectors neural DTC

Fig. 17. Results of the fourth empirical test.

Furthermore, it is noted that a change in speed value directly affects the period of the current signal for the two controls. At low speeds, the period value increases significantly for the two techniques. On the other hand, it is noted that current ripples increase significantly at low speeds for the two controls. Therefore, it can be said that low speed affects current quality. Therefore, low-speed operation can be considered one of the most significant drawbacks of the traditional and proposed approaches.

Figure 18 represents the THD of current for the two controls in the fourth test. This value was 17.39 % for the conventional approach and 9.12 % for the proposed 12 sectors neural DTC approach. Therefore, the proposed approach yielded a THD value significantly lower than that obtained by the conventional method. The proposed approach reduced the THD value at low speed by a percentage of 47.56 %. This percentage demonstrates the effectiveness of the designed 12 sectors neural DTC approach and its ability to reduce THD despite the lower rotational speed compared to the conventional approach. On the other hand, Figure 18 shows that the fundamental signal (50 Hz) amplitude was 3.28 A for the conventional 6 sectors DTC approach and 3.29 A for the proposed 12 sectors neural DTC approach. These values demonstrate the effectiveness of the designed approach in improving the amplitude value compared to the conventional approach. These obtained results highlight the effectiveness, efficiency, and high operational performance of the designed 12 sectors neural DTC approach, making it a reliable solution for other industrial applications such as electric vehicles and renewable energy.

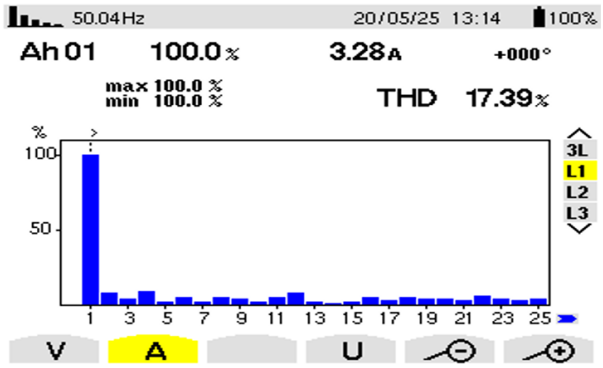

(a) DTC

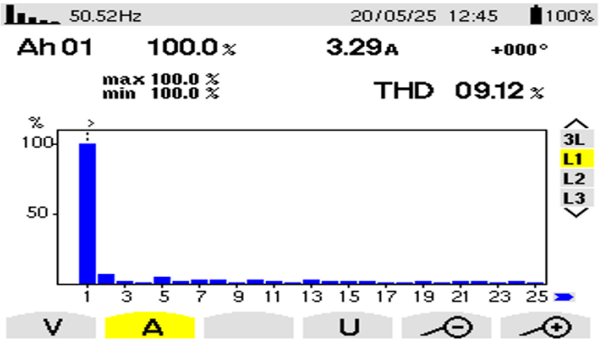

(b) 12 sectors neural DTC

Fig. 18. Current THD (fourth empirical test).

Table 11 compares the proposed strategy with related works in terms of the THD value of current data. This comparison highlights the effectiveness of the proposed 12 sectors neural DTC approach in providing a significantly better value than several related scientific works. Based on this table, the designed approach reduced the THD value by 26.24 %, 17.47 %, and 46.95% compared to the fuzzy predictive control strategy [52], fuzzy DTC approach [54], and seven-level neural DTC with fuzzy speed controller [56], respectively.

The designed strategy reduced the THD value by 5.92%, 24.19 %, 85.61%, and 27.47 % compared to the neural DTC technique [30], Conventional SMC–based DTC-SVM scheme [58], 12 sectors DTC based on super-twisting controllers [59], and neuro-fuzzy DTC technique [55], respectively.

These ratios highlight the effectiveness of the designed approach in reducing the THD of current compared to several strategies found in the literature, such as the 12-sector DTC based on super-twisting controllers and the conventional SMC–based DTC-SVM scheme. This comparison demonstrates that the designed approach has a significant potential to improve current quality, making it a promising and reliable solution for electric vehicles and renewable energy (wind energy).

On the other hand, the work designed in this paper is compared with the work completed in [60, 61], as this comparison aims to highlight the importance of the work completed compared to several works found in the literature.

Table 11. Comparison with other related works in terms of current THD value.

References and techniques			THD (%)
[30]		Neural DTC technique	6.93
		Tree DTC technique	6.60
		Traditional DTC strategy	11.78
[50]		Optimized stator flux reference by TOA method	7.20
[51]		Neural network method	22.48
[52]		Fuzzy predictive control	8.84
[53]	Low speed	Traditional DTC technique	9.30
		Fuzzy DTC technique	7.90
	High speed	Traditional DTC technique	9.10
		Fuzzy DTC technique	7.50
[54]		Traditional DTC technique	9.30
		Fuzzy DTC technique	7.90
		Optimized DTC strategy	7.30
[55]		Neuro-fuzzy DTC technique	8.99
[56]		Seven-level DTC technique	26.92
		Seven-level neural DTC with fuzzy speed controller	12.29
[57]		Standard DTC	7.27
		DTC technique with ramp modulator	7.10
[58]		DTC-SVM with single PI controller	13.85
		Conventional SMC–based DTC-SVM scheme	8.60
[59]		Basic DTC technique	76.92
		12 sectors DTC based on super-twisting controllers	45.30
Proposed technique			6.52

In the study by J. Park, et al. ("Direct Torque Control in PMSM Using a 12-Segment Approach and Pulse Width Modulation Based on the Supplied Voltage Function," 2018) [60], a 12-segment DTC scheme coupled with pulse width modulation is implemented for the PMSM, using constant switching logic and voltage vector selection rules. In contrast, our work focuses on an inductive (asynchronous) machine instead of a PMSM, replacing the fixed comparator/switchable structure with a neural network decision unit, enabling adaptive mapping of flow/torque error signals and sector information for voltage vector selection. While J. Park et al.'s approach aims to improve vector modification and switching behavior within a 12-segment framework, it retains the classical rationale; our approach develops this by adopting machine learning-based reasoning for the switching decision and demonstrates full experimental implementation rather than just simulation.

The second reference study, conducted by A. Pal, et al. [61], applies torque comparison (DTC) to a 12-segment induction motor in the simulation by increasing the levels of the comparator (a five-level torque comparator) and thus improving the accuracy of the hysteresis switching. While it improves upon classical hysteresis comparison tables and comparisons, it remains within the traditional hysteresis + search table model and is limited to simulation. Our proposed work deviates from this by eliminating hysteresis comparisons and completely replacing the switching table with a neural network for voltage vector selection, and by providing real-time experimental verification on hardware.

Taken together, while reference works drive incremental improvements to the 12-sector DTC architecture (via enhanced comparison levels or PWM modulation) within the framework of the traditional logic table, our designed work transforms the model into an adaptive neural-based selection mechanism, extends the application to induction machines, and demonstrates practical device performance gains (e.g., lower torque ripple, faster transient response) that go beyond the simulation-only context of previous studies.

7. Conclusions

This work discusses the application of neural algorithms to address the issues associated with traditional direct torque control techniques. The algorithm was initially implemented in MATLAB with various tests, and its results were compared to those of the traditional 6 sectors DTC approach. Subsequently, an experimental implementation of the proposed algorithm was conducted using real equipment based on dSPACE 1104. Three different tests were proposed to evaluate the efficiency and effectiveness of the 12-sector neural DTC strategy in comparison to the traditional 6-sector DTC technique. The experimental results confirmed the simulation outcomes, demonstrating the competence and capabilities of the 12 sectors of the neural DTC technique in enhancing the proposed control system. The findings indicate that the suggested algorithm effectively overcomes the challenges posed by the traditional 6 sectors' DTC method. Key results from the experimental work can be summarized as follows:

- An improved dynamic speed response by 47% compared to the traditional 6 sectors DTC technique.
- A significant reduction in the incidence of exceeding the speed limit.
- Decreased fluctuations in current, torque, and flux compared to the traditional 6 sectors DTC method.
- A 30.87%, 42.22%, and 49.73% reduction in the THD of current, relative to the traditional 6 sectors DTC technique.

These experimental results highlight the effectiveness of utilizing a neural algorithm to overcome the limitations of the traditional DTC approach. This algorithm has potential applications in various sectors, including factories producing electric motors, where it can serve as an effective tool for controlling electrical machines. In the industrial sector, the proposed algorithm could enhance the power quality and current stability of large generators used in offshore wind turbines and hydro pumps. Unlike strategies that rely on mathematical modeling of the studied system—which can

increase vulnerability to changing system parameters—the designed algorithm is characterized by its simplicity and does not rely on mathematical modeling of the system being studied. This simplicity underscores the importance of the proposed algorithm for future applications in other fields.

In the future, additional experimental work will be conducted on the DTC technique for the AM drive algorithm, employing nonlinear strategies such as the SMC approach or BC technique, with results compared to those obtained from the algorithm proposed in this work.

Nomenclature

DTC	Direct torque control
NN	Neural network
SMC	Sliding mode controller
PI	Proportional-integral controller
EM	Electrical machine
HC	Hysteresis comparator
MM	Mathematical model
MRAC	Model reference adaptive control
WT	Wind turbine
SPWM	Sinusoidal pulse width modulation
VFD	Variable frequency drive
AM	Asynchronous machine
THD	Total harmonic distortion
GA	Genetic algorithm
RE	Renewable energy
FOC	Field-oriented control
ST	Switching table
SVM	Space vactor modulation
BC	Backstepping control
ACO	Ant colony optimization
FSOSMC	Fuzzy second-order sliding mode controller
MPPT	Maximum power point tracking
SF	Switching frequency

Author Contributions

Conceptualization: H.B., A.Y., and A.M.; Methodology: H.B., A.Y., A.M., and N.B.; Software: H.B. and A.M.; Validation: H.B. and A.M.; Formal analysis: A.Y., A.M., H.B., and N.B.; Investigation: A.M., H.B., and N.B.; Resources: A.M. and H.B.; Data curation: A.Y., A.M., and H.B.; Writing—original draft preparation: A.Y., A.M., and H.B.; Writing—review and editing: A.M., H.B., and N.B.; Visualization: A.M., A.Y., H.B., and N.B.; Supervision: A.Y., A.M., H.B., and N.B.; Project administration: A.M. and H.B.; Funding acquisition: A.M. and H.B. All authors have read and agreed to the published version of the manuscript.

Acknowledgements

Conflict of Interest

The authors declare no conflict of interest.

References

[1] I. Takahashi, T. Noguchi, “A new quick-response and high-efficiency control strategy of an induction motor,” IEEE Transactions on Industry Applications, vol. 5, pp. 820–827, 1986.

[2] A. Ammar, B. Talbi, T. Ameid, Y. Azzoug, A. Kerrache, “Predictive direct torque control with reduced ripples for induction motor drive based on T-S fuzzy speed controller,” Asian Journal of Control, vol. 21, No. 4, pp. 2155–2166, 2019.

[3] N. El Ouanjli, A. Derouich, A. El Ghzizal, S. Motahhir, A. Chebabhi, Y. El Mourabit, M. Taoussi, “Modern improvement techniques of direct torque control for induction motor drives-a review,” Protection and Control of Modern Power Systems, vol. 4, No. 1, pp. 1–12, 2019.

[4] T. Sutikno, N. R. N. Idris, A. Jidin, “A review of direct torque control of induction motors for sustainable reliability and energy efficient drives,” Renewable and Sustainable Energy Reviews, vol. 32, pp. 548–558, 2014.

[5] S. El Daoudi, L. Lazrak, N. El Ouanjli, M. A. Lafkih, “Sensorless fuzzy direct torque control of induction motor with sliding mode speed controller,” Computers and Electrical Engineering, vol. 96, pp. 107490, 2021.

[6] A. Ammar, A. Bourek, A. Benakcha, “Nonlinear SVM-DTC for induction motor drive using input-output feedback linearization and high order sliding mode control,” ISA Transactions, vol. 67, pp. 428–442, 2017.

[7] S. Jadhav, K. Jaladi, “Advanced VSC and intelligent control algorithms applied to SVM-DTC for induction motor drive: A comparative study,” 2016 12th World Congress on Intelligent Control and Automation (WCICA), IEEE, pp. 2694–2698, 2016.

[8] S. El Daoudi, L. Lazrak, B. El Ouanjli, M. Ait Lafkih, “Applying sliding mode technique for the nonlinear DTC-SPWM control strategy of sensorless squirrel cage asynchronous motor,” International Journal of Dynamics and Control, vol. 9, No. 4, pp. 1633–1644, 2021.

[9] E. Najib, M. Said, A. Ameena Saad, E. Soukaina, D. Aziz, E. Mohammed, “Improved twelve sectors DTC strategy of induction motor drive using Backstepping speed controller and P-MRAS stator resistance identification-design and validation,” Alexandria Engineering Journal, vol. 80, pp. 358–371, 2023, Doi: 10.1016/j.aej.2023.08.077.

[10] M. Said, D. Aziz, I. Atif, E. Najib, “ANT-colony optimization-direct torque control for a doubly fed induction motor: An experimental validation,” Energy Reports, vol. 8, pp. 81–98, 2022, Doi: 10.1016/j.egyr.2021.11.239.

[11] M. Dursun, “Enhancement fractional-order sliding mode controller design for induction motor vector control,” Iranian Journal of Science and Technology, Transactions

of Electrical Engineering, vol. 47, pp. 1059–1080, 2023, Doi: 10.1007/s40998-023-00637-2.

[12] S. Sharma, B. Singh, A. Datar, "Duty ratio control technique with torque ripple minimization for induction motor-based electric vehicle applications," Journal of Power Electronics, vol. 23, pp. 617–624, 2023, Doi: 10.1007/s43236-023-00595-2.

[13] A. K. Sahoo, R. K. Jena, "Reduction of torque ripple in induction motor-driven electric vehicle using optimized stator flux," International Journal of Information Technology, vol. 15, pp. 1333–1346, 2023, Doi: 10.1007/s41870-023-01172-3.

[14] G. Boukhalfa, S. Belkacem, A. Chikhi, "Fuzzy-second order sliding mode control optimized by genetic algorithm applied in direct torque control of dual star induction motor," Journal of Central South University, vol. 29, pp. 3974–3985, 2022, Doi: 10.1007/s11771-022-5028-3.

[15] S. Siliveru, N. R. Reddy, "Comparative switching and conduction loss analysis of a SVPWM and DPWM based DTC of open end winding induction motor drive," International Journal of Renewable Energy Research, vol. 12, No. 4, pp. 1954–1965, 2022, Doi: 10.20508/ijrer.v12i4.13466.g8618.

[16] G. Goksel, A. K. Ahmet, "Design and implementation of a wind turbine emulator using an induction motor and direct current machine," International Journal of Renewable Energy Research, vol. 10, No. 3, pp. 1426–1438, 2020, Doi: 10.20508/ijrer.v10i3.10723.g8018.

[17] C. Ghizlane, M. Zakaria, A. Abdelouahed, M. Mustapha, "Speed control of induction motor driving a pump supplied by a photovoltaic array," International Journal of Renewable Energy Research, vol. 10, No. 1, pp. 237–242, 2020, Doi: 10.20508/ijrer.v10i1.10320.g7859.

[18] S.F.A. Bukhari, H. Kahveci, M. E. Şahin, "Single Phase Induction Motor Driver for Water Pumping Powered by Photovoltaic System," Electronics vol. 14, No. 16, pp. 1189, 2025. Doi: 10.3390/electronics14061189.

[19] M. F. Masood, I. A. Muhammad, S. K. Muhammad, M. Tasawar, A. R. Muhammad, H. Ur Rehman, Z. Tausif, "A novel solution to eliminate frequency intermittency by adding spinning reserve to the micro-hydro turbine generator using real-time control of induction motor through AC-DC-AC power converters," International Journal of Smart Grid, vol. 4, No. 4, pp. 149–156, 2020, Doi: 10.20508/ijsmartgrid.v4i4.120.g106.

[20] P. P. Vinodkumar, T. Prashant, Z. Pankaj, "Hardware Implementation and Closed Loop Simulation of SPWM and PI based Hybrid Control for Matrix Converter fed Single Phase Induction Motor Powered by PV system," International Journal of Renewable Energy Research-IJRER vol. 13, no. 4, pp. 1481-1496, 2023. https://doi.org/10.20508/ijrer.v13i4.14001.g8822.

[21] P. Aurobinda, K. P. Mukesh, P. S. Satya, "Solar direct torque controlled induction motor drive for industrial applications," International Journal of Renewable Energy Research, vol. 3, No. 4, pp. 794–802, 2013, Doi: 10.20508/ijrer.v3i4.848.g6207.

[22] H. Benbouhenni, Z. Boudjema, "Two-level DTC based on ANN controller of DFIG using 7-level hysteresis command to reduce flux ripple comparing with traditional command," 2018 International Conference on Applied Smart Systems (ICASS), Medea, Algeria, pp. 1–8, 2018, Doi: 10.1109/ICASS.2018.8652013.

[23] H. Benbouhenni, Z. Boudjema, "Speed regulateur and hysteresis based on artificial intelligence techniques of three-level DTC for induction motor," Acta Electrotechnica et Informatica, vol. 17, No. 4, pp. 48–54, 2017.

[24] A. Milles, H. Benbouhenni, N. Bensedira, "Experimental verification of the six sectors neural DTC approach of squirrel cage induction motors," Scientific Reports, vol. 15, pp. 10787, 2025, Doi: 10.1038/s41598-025-95333-y.

[25] B. Habib, "Rotor flux and electromagnetic torque regulation of DFIG using dual PI controllers," International Journal of Smart Grid, vol. 7, No. 4, pp. 227–234, 2023, Doi: 10.20508/ijsmartgrid.v7i4.308.g311.

[26] B. Habib, "Stator current and rotor flux ripples reduction of DTC DFIG drive using FSTSMC algorithm," International Journal of Smart Grid, vol. 3, No. 4, pp. 226–234, 2019, Doi: 10.20508/ijsmartgrid.v3i4.82.g72.

[27] B. Habib, "Utilization of an ANFIS-STSM algorithm to minimize total harmonic distortion," International Journal of Smart Grid, vol. 4, No. 2, pp. 56–67, 2020, Doi: 10.20508/ijsmartgrid.v4i2.98.g82.

[28] K. K. Danduprolu, R. D. G. Tulasi, "Fuzzy logic controller based performance of SPMSM fed with improved direct torque control," International Journal of Renewable Energy Research, vol. 9, No. 3, pp. 1346–1354, 2019, Doi: 10.20508/ijrer.v9i3.9625.g7714.

[29] A. Sahu, B. M. Kanungo, N. M. Rabi, "Development and experimental realization of an adaptive neural-based discrete model predictive direct torque and flux controller for induction motor drive," Applied Soft Computing, vol. 108, pp. 107418, 2021, Doi: 10.1016/j.asoc.2021.107418.

[30] A. Oualid, R. Abderrahim, K. Abdelbasset, B. Rabah, T. Hicham, A.-R. Haitham, "Advanced direct torque control based on neural tree controllers for induction motor drives," ISA Transactions, vol. 148, pp. 92–104, 2024, Doi: 10.1016/j.isatra.2024.03.017.

[31] G. Soufien, M. Abdellatif, F. M. Mohamed, "Artificial neural network-based DTC of an induction machine with experimental implementation on FPGA," Engineering Applications of Artificial Intelligence, vol. 121, pp. 105972, 2023, Doi: 10.1016/j.engappai.2023.105972.

[32] X. Liu, C. Zhang, K. Li, "Neural network-based direct torque control of PMSM with reduced torque ripple,"

IEEE Transactions on Industrial Electronics, vol. 66, No. 11, pp. 8638–8647, 2019.

[33] Y. Zhang, J. Zhu, W. Xu, "Direct torque control of induction motors using an artificial neural network," IEEE Transactions on Power Electronics, vol. 26, No. 2, pp. 580–588, 2011.

[34] J. Hu, W. Xu, L. Huang, "Adaptive neural network-based direct thrust control for linear induction motor drives," IEEE Transactions on Industrial Electronics, vol. 65, No. 12, pp. 9926–9935, 2018.

[35] M. A. Khan, M. A. Rahman, "FPGA-based neural network controller for direct torque control of IM," IEEE Transactions on Industrial Informatics, vol. 13, No. 3, pp. 1172–1181, 2017.

[36] F. Wang, S. Li, X. Mei, "Deep reinforcement learning-based direct torque control for PMSM with parameter robustness," IEEE Transactions on Power Electronics, vol. 35, No. 7, pp. 7341–7352, 2020.

[37] M. Abderrahmane, B. A. Djilani, B. Habib, B. Youcef, N. Benharir, Z. M. S. Elbarbary, "Enhanced direct torque control based on intelligent approach for doubly-fed induction machine fed by three-level inverter," Heliyon, vol. 10, No. 21, pp. e39738, 2024, Doi: 10.1016/j.heliyon.2024.e39738.

[38] A. El Idrissi, A. Derouich, S. Mahfoud, N. El Ouanjli, H. Chojaa, A. Chantoufi, "Bearing faults diagnosis by current envelope analysis under direct torque control based on neural networks and fuzzy logic—A comparative study," Electronics, vol. 13, pp. 3195, 2024, Doi: 10.3390/electronics13163195.

[39] M. A. Khan, B. Asad, T. Vaimann, A. Kallaste, "An advanced diagnostic approach for broken rotor bar detection and classification in DTC controlled induction motors by leveraging dynamic SHAP interaction feature selection (DSHAP-IFS) GBDT methodology," Machines, vol. 12, pp. 495, 2024, Doi: 10.3390/machines12070495.

[40] L. P. Chisedzi, M. Muteba, "Detection of broken rotor bars in cage induction motors using machine learning methods," Sensors, vol. 23, pp. 9079, 2023, Doi: 10.3390/s23229079.

[41] H. Benbouhenni, N. Bizon, I. Colak, M. Iliescu, P. Thounthong, "A new direct torque control of an efficient and cost-effective traction system using two squirrel cage induction motors fed by a single inverter," Electric Power Components and Systems, In Press, pp. 1–21, 2024, Doi: 10.1080/15325008.2024.2325541.

[42] N. H. Viet, N. Paraschiv, "An investigation on twelve sectors direct torque control for induction motors fed by matrix converter," 2020 12th International Conference on Electronics, Computers and Artificial Intelligence (ECAI), Bucharest, Romania, pp. 1–5, 2020, Doi: 10.1109/ECAI50035.2020.9223148.

[43] S. Younes, T. Salah, L. B. Sofia, B. Mohit, B. Youcef, R. S. Arvind, F. E. Mohamed, K. Salah, "Effectiveness analysis of twelve sectors of DTC based on a newly modified switching table implemented on a wind turbine DFIG system under variable wind velocity," Ain Shams Engineering Journal, vol. 14, No. 11, pp. 102221, 2023.

[44] M. Jafari, K. Abbaszadeh, M. A. Mohammadian, "A 12-sector space vector switching table for parallel-connecting to dual induction motors fed by matrix convertor based on direct torque control," SN Applied Sciences, vol. 3, pp. 849, 2021, Doi: 10.1007/s42452-021-04763-6.

[45] H. Albalawi, S. A. Zaid, M. E. El-Shimy, A. M. Kassem, "Ant colony optimized controller for fast direct torque control of induction motor," Sustainability, vol. 15, pp. 3740, 2023, Doi: 10.3390/su15043740.

[46] S. Krim, S. Gdaim, A. Mtibaa, M. F. Mimouni, "Modeling and hardware implementation on the FPGA of a variable structure control associated with a DTC-SVM of an induction motor," Electric Power Components and Systems, vol. 45, No. 16, pp. 1806–1821, 2017, Doi: 10.1080/15325008.2017.1351010.

[47] B. Habib, Z. Dalal, "Neural modified super-twisting filed-oriented approach of asynchronous machine drives," Artificial Intelligence Research and Applications, vol. 1, No. 1, pp. 1–18, 2025, Doi: 10.20508/ijaira/n32q3x57.

[48] B. Habib, "Application of five-level NPC inverter in DPC-ANN of doubly fed induction generator for wind power generation systems," International Journal of Smart Grid, vol. 3, No. 3, pp. 128–137, 2019, Doi: 10.20508/ijsmartgrid.v3i3.66.g59.

[49] M. Keddar, L. D. Mamadou, D. Mohamed, B. Karim, M. Abdelhami, "Interconnection performance analysis of single phase neural network based NPC and CHB multilevel inverters for grid-connected PV systems," International Journal of Renewable Energy Research, vol. 9, No. 3, pp. 1451–1461, 2019, Doi: 10.20508/ijrer.v9i3.9593.g7730.

[50] X. Sun, J. Wu, G. Lei, Y. Guo, J. Zhu, "Torque ripple reduction of SRM drive using improved direct torque control with sliding mode controller and observer," IEEE Transactions on Industrial Electronics, vol. 68, pp. 9334–9345, 2021, Doi: 10.1109/TIE.2020.3020026.

[51] K. Bouhoune, K. Yazid, M. S. Boucherit, B. N. Mobarakeh, "Simple and efficient direct torque control of induction motor based on artificial neural networks," Proceedings of the IEEE International Conference on Electrical Systems for Aircraft, Railway, Ship Propulsion and Road Vehicles & International Transportation Electrification Conference, pp. 1–6, 2018, Doi: 10.1109/ESARS-ITEC.2018.8607747.

[52] A. Berzoy, J. Rengifo, O. Mohammed, "Fuzzy predictive DTC of induction machines with reduced torque ripple and high-performance operation," IEEE Transactions on

Power Electronics, vol. 33, pp. 2580–2587, 2018, Doi: 10.1109/TPEL.2017.2690405.

[53] K. S. Anjan, K. J. Ranjan, "Improved DTC strategy with fuzzy logic controller for induction motor driven electric vehicle," AIMS Electronics and Electrical Engineering, vol. 6, No. 3, pp. 296–316, 2022, Doi: 10.334/electreng.2022018.

[54] K. S. Anjan, K. J. Ranjan, "Teamwork optimization based DTC for enhanced performance of IM based electric vehicle," Turkish Journal of Electrical Engineering & Computer Sciences, vol. 31, No. 2, pp. 360–380, 2023, Doi: 10.55730/1300-0632.3989.

[55] A. Oualid, R. Abderrahim, T. Hicham, Z. Djamel, S. Abdelhakim, "An improved direct torque control with an advanced broken-bar fault diagnosis for induction motor drives," International Transactions on Electrical Energy Systems, vol. 2023, pp. 1–18, 2023, Doi: 10.1155/2023/8816896.

[56] B. Habib, "Seven-level direct torque control of induction motor based on artificial neural networks with regulation speed using fuzzy PI controller," Iranian Journal of Electrical and Electronic Engineering, vol. 14, No. 1, pp. 85–94, 2018.

[57] E. E. El-Kholy, S. Mahmoud, R. Kennel, A. El-Refaei, F. Elkady, "Torque ripple minimization for induction motor drives with direct torque control," Electric Power Components and Systems, vol. 33, No. 8, pp. 845–859, 2005, Doi: 10.1080/15325000590909804.

[58] S. K. Gudey, M. Malla, K. Jasthi, S. R. Gampa, "Direct torque control of an induction motor using fractional-order sliding mode control technique for quick response and reduced torque ripple," World Electric Vehicle Journal, vol. 14, pp. 137, 2023, Doi: 10.3390/wevj14060137.

[59] Z. Yassine, M. Mohamed, T. Souad, F. Chaymae, E. Sara, "Induction motor performance improvement using super twisting SMC and twelve sector DTC," International Journal of Robotics and Control Systems, vol. 4, No. 1, pp. 50–68, 2024, Doi: 10.31763/ijrcs.v4i1.1090.

[60] J. Park, J.-W. Kim, D.-H. Lee, "Direct torque control of PMSM using 12-sector and PWM approach based on the supplied voltage function," 2018 10th International Conference on Information Technology and Electrical Engineering (ICITEE), Bali, Indonesia, pp. 476–481, 2018, Doi: 10.1109/ICITEE.2018.8534831.

[61] A. Pal, G. D. Srivastava, R. D. Kulkarni, "Simulation of sensorless speed control of induction motor using direct torque control technique employing five level torque comparator and twelve sector method," 2019 International Conference on Nascent Technologies in Engineering (ICNTE), Navi Mumbai, India, pp. 1–6, 2019, Doi: 10.1109/ICNTE44896.2019.8945936.